AN INTEGRATED APPROACH TO DETERMINE PHENOMENOLOGICAL EQUATIONS IN METALLIC SYSTEMS

Iman Ghamarian, B.S.

Thesis Prepared for the Degree of

MASTER OF SCIENCE

UNIVERSITY OF NORTH TEXAS

December 2012

APPROVED:

Peter C. Collins, Major Professor
Rajarshi Banerjee, Committee Member
Zhiqiang Wang, Committee Member
Narendra Dahotre, Chair of the Department of Materials Science and Engineering
Costas Tsatsoulis, Dean of the College of Engineering
Mark Wardell, Dean of the Toulouse Graduate School

Ghamarian, Iman, An Integrated Approach to Determine Phenomenological Equations in Metallic Systems. Master of Science (Materials Science and Engineering), December 2012, 58 pp., 23 figures, 4 tables, references, 40 titles.

It is highly desirable to be able to make predictions of properties in metallic materials based upon the composition of the material and the microstructure. Unfortunately, the complexity of real, multi-component, multi-phase engineering alloys makes the provision of constituent-based (i.e., composition or microstructure) phenomenological equations extremely difficult. Due to these difficulties, qualitative predictions are frequently used to study the influence of microstructure or composition on the properties. Neural networks were used as a tool to get a quantitative model from a database. However, the developed model is not a phenomenological model. In this study, a new method based upon the integration of three separate modeling approaches, specifically artificial neural networks, genetic algorithms, and monte carlo was proposed. These three methods, when coupled in the manner described in this study, allows for the extraction of phenomenological equations with a concurrent analysis of uncertainty. This approach has been applied to a multi-component, multi-phase microstructure exhibiting phases with varying spatial and morphological distributions. Specifically, this approach has been applied to derive a phenomenological equation for the prediction of yield strength in $\alpha+\beta$ processed Ti-6-4. The equation is consistent with not only the current dataset but also, where available, the limited information regarding certain parameters such as intrinsic yield strength of pure hexagonal close-packed alpha titanium.

ACKNOWLEDGEMENTS

First and foremost, I wish to express my deep sense of gratitude to my advisor, Dr. Peter Collins, for his outstanding, endless support to my academic as well as personal life. He is an infinite source of encouragement and motivation. His pristine ideas and vital suggestions played a key role in my research. I highly appreciate him for his brilliant patience and effort to help me reach my dreams and I do know that I owe him a lot.

I would like to thank my committee members Dr. Rajarshi Banerjee, for his helps and supports on the thesis, and Dr. Zhiqiang Wang, for his comments on my thesis.

I am also grateful to Ankit Srivastava for great discussions we had, to conduct the project and Vaibhav Gupta with whom I started the project. I learnt a lot from both of them. I like to thank my group mates and MTSE staffs who helped me many times during the past two years.

Last but not least, I would like to express my genuine gratitude to my parents, Nasir and Monir, whose continuous supports and kindness help and motivate me to progress in my life and proceed my educations.

To Pete, who taught me well the meaning of the words “Persistence” and “Perseverance”

TABLE OF CONTENTS

Page

LIST OF TABLES

Page

LIST OF FIGURES

Page

CHAPTER 1

INTRODUCTION

1.1 Motivation

It is highly desirable to be able to make predictions of properties in metallic materials based upon the composition and microstructure of the material. Unfortunately, the complexity of real, multi-component, multi-phase engineering alloys often makes the provision of constituent-based (i.e., composition or microstructure) phenomenological equations extremely difficult. Therefore, qualitative predictions are frequently used to study the influence of microstructure or composition on the properties (Table 1.1). Neural networks (NN) have been used as a tool to derive a quantitative model from a database. However, the developed model is not a traditional phenomenological model. In this thesis, a new method based upon the integration of three separate modeling approaches, specifically artificial neural networks, genetic algorithms (GA), and Monte Carlo (MC) is proposed. These three methods, when coupled in the manner described in this study, allows for the extraction of phenomenological equations with a concurrent analysis of uncertainty. This approach has been applied to a multi-component, multi-phase microstructure exhibiting phases with varying spatial and morphological distributions.

Specifically, it has been applied to derive a phenomenological equation for the prediction of yield strength in $\alpha+\beta$ processed Ti-6-4. The equation is consistent with not only the current dataset but also, where available, the limited information regarding certain parameters such as intrinsic yield strength of pure hexagonal close-packed alpha titanium and the potency of solid solution strengthening in titanium and its alloys.

Table 1.1. Qualitative mechanical property predictions [1]

α +β titanium alloys	σ_y	ε_F	High-cycle-fatigue	Micro cracks da/dN	Macro-cracks ΔK_{th}		K_{IC} ΔK_{th}	Creep strength 0.2%
Aging (α2) Oxygen	+	-	+	-	-	-	+	+
Bi-modal structure	+	+	-/+	+	-	-	-	-/0
GB α-layer	0	-	-	-	0	-	0	0
Small α-colonies	+	+	+	+	-	-	-	-

1.2 Scope of the Current Work

The benefits, include, for example, a reduction in design time, an improvement in the understanding of material allowables, and the direct of determination of phenomenological equations. However, the desire to have such phenomenological equations has often been impeded by the limitations of both experimental and computational approaches. For example, there have been great advances in the ability to predict elastic properties in complex multi-phase alloys. Similarly, there have been great advances to predict the elastic-plastic behavior in single-phase materials. However, the approaches to predict elastic-plastic properties of multi-phase can often be elusive as a phenomenological equation or components thereof are requisite inputs. Regarding experimentation, it is often the case that the microstructural features relevant to the mechanical properties are numerous and are themselves interrelated, often rendering the experimental isolation of a single variable, and therefore the direct assessment of portions of a phenomenological equation, impossible.

A wide variety of titanium alloys represents a very good example. Consider the microstructure shown in fig. 1.1 of an α+β processed alloy Ti-6-4 (nominally cited as Ti-6Al-

4V, but whose actual composition can vary significantly, see Table 1.2). This material, once subjected to mechanical working at elevated temperatures high in the α+β two-phase field followed by cooling and aging, exhibits a complex microstructure comprised of two phases, the hexagonal close packed (hcp) alpha phase and the body centered cubic (bcc) β-phase. Further, the hcp alpha phase presents two distinct morphologies and exhibit a range of feature length scales. The first morphology, the coarser feature, is often called equiaxed alpha. This particular morphology does not necessarily share the traditional hcp/bcc Burger's orientation relationship. The second morphology is the finer feature and is designated as laths. This latter morphology, the α-laths, does exhibit a Burger's orientation relationship with the bcc beta phase. In addition, as is well known in titanium metallurgy, the Al and O will preferentially partition to the alpha phase, and the V and Fe will preferentially partition to the beta phase. Clearly, the microstructure is quite complex.

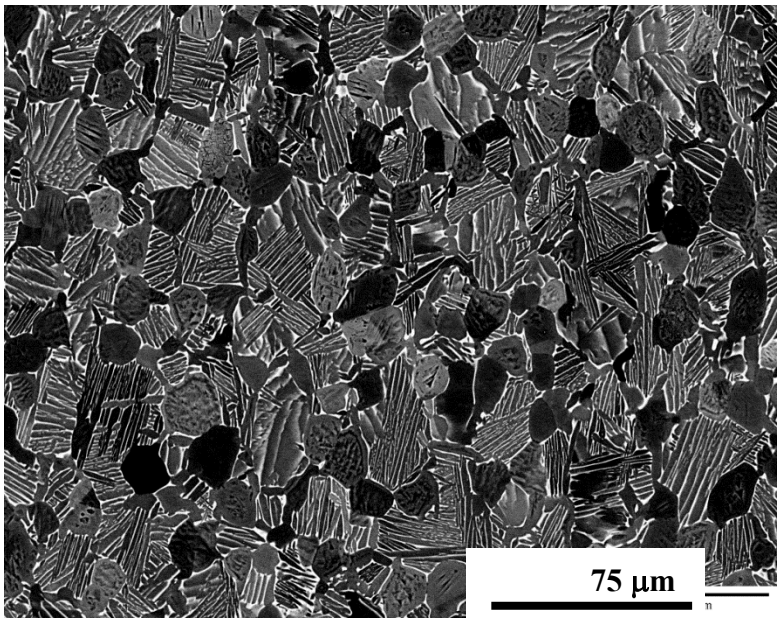

Figure 1.1.A typical microstructure of α/β processed Ti-6Al-4V is shown. This backscattered SEM micrograph shows both equiaxed and lamellar α-features (darker phase) and the β phase (light)

Table 1.2. Composition range of Ti-6Al-4V alloy [2]

Element	Composition range (wt%)
Al	5.5-6.75
V	3.5-4.5
Fe	0-0.3
O	0-0.2

Consider fig. 1.2, which shows three different alloys which all fall within (or exceptionally close to) the specifications of Ti-6Al-4V, but for which the clearly observable differences in microstructure and composition contribute to the yield strength in offsetting fashions. In other words, these materials exhibit nominally identical yield strengths. While fig. 1.2 clearly illustrates the problem, it is also demonstrated very nicely in the work of Kar et al. [3] who point out the natural scatter in the data when only considering one variable, and note the great difficulty that one would face attempting to extract a direct relationship. Their solution to the problem, and one adopted in other similar work [4-8] is to use artificial neural networks, such as those based upon Bayesian statistics [9-12] , to formulate the interrelationships that exist among the various input variables. These efforts have been notable in their ability to make interpolative predictions of yield strength [13, 14] and, as yet unpublished, fracture toughness. Further, significant progress is presented in these papers as the concept of virtual experiments were introduced as a way to assess the relative influence of input variables on the output, in these cases yield strength. However, the architecture of neural networks can be complex, as is shown in chapter 2.

Herein lies the problem. While the equation given by a neural network may be generally valid for the particular dataset for which the physics are unknown and the interrelations complex, the incorporation of weights and the flexible hyperbolic tangent function, once extracted, does not appear to possess the same forms as would be expected were the physics to be known.

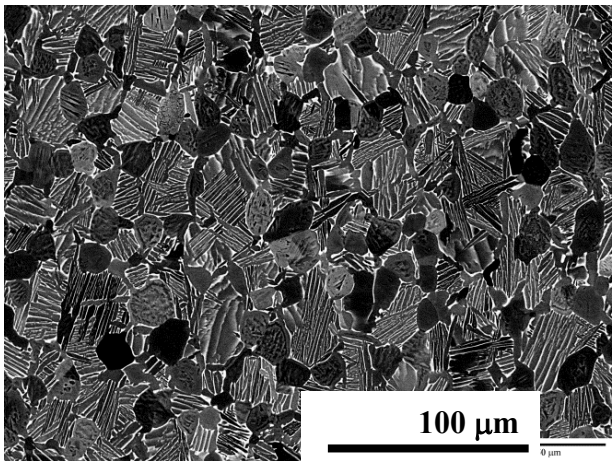

(a)

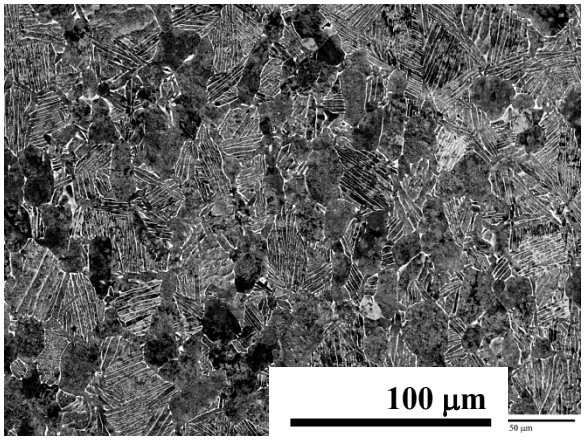

(b)

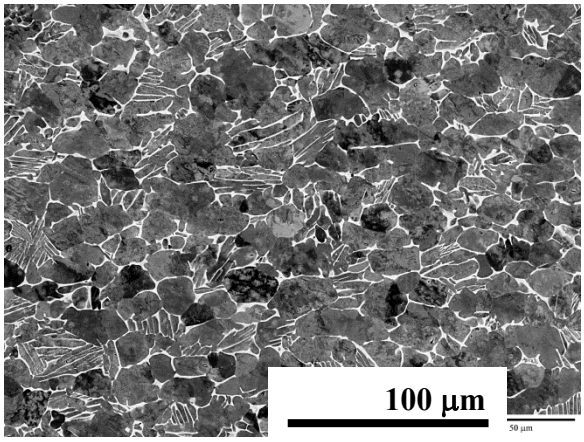

(c)

Figure 1.2. Influences of microstructure and composition on yield strengthis shown. (a) The yield strength for this given microstructure and composition (Ti-6.55Al-4.38V-0.41Fe-0.197O (wt%)) is 844 MPa, (b) The yield strength for Ti-4.766Al-3.297V-0.11Fe-0.08O (wt%) is 846 MPa. Influences of microstructure and composition on yield strengthis shown. (c) The yield strength for Ti-6.514Al-4.45V-0.11Fe-0.079O (wt%) is 845 MPa.

For example, consider a very simple problem, namely the influence of grain size on yield strength in a single phase bcc crystal for which there is a strong influence of grain size on yield strength. Classically, we understand the classical problem as best represented as the "Hall-Petch" relationship [15-18], and a resulting equation may take the form of equation 1.3, where the design property (yield strength, σ_{ys}) is related to the intrinsic strength of the material (σ_0), a material constant (k_y) and grain diameter (d).

$$\sigma_{ys} = \sigma_0 + \frac{k_y}{d^{-0.5}} \qquad \textbf{Eq. 1.3}$$

This equation is rooted in dislocation theory, and takes a form where the physics likely have been directly, albeit perhaps simply, captured. In other words, based upon our understanding of materials, the equation is one we can understand rationally with respect to operating mechanisms. A summation of weighted hyperbolic tangent functions, while mathematically accurate for a given dataset, can neither be understood as instinctively nor correlated with the physics of the problem. This reality is concurrently both the prime motivation for the use of neural networks (the physics need not be understood) and the cause for suspicion in their broad exploitation (the physics are not illuminated).

While artificial neural networks have, over the years, increasingly gained acceptance as a tool to provide predictive tools for various aspects of materials science, genetic algorithms have largely been ignored. Indeed, although Bhadeshia explored briefly the use of genetic algorithms and found them to be less effective than neural networks [19], few other have even considered their application to materials science.

Genetic algorithms are highly flexible optimization tools that search for the global minimum or maximum of a numerically defined problem. Most often, the problem takes the form of a function or a solution to a large database search where fitness can be numerically

defined. The strategy that genetic algorithms use is analogous to natural selection. The algorithm continually and repeatedly modifies a population of individual solution strings. For every step, the algorithm selects the "fittest" individual solution strings (based upon selection rules). These solution strings are then "parents" and used to produce the next generation of potential solution strings. Over successive "generations" (i.e., algorithm iterations), the overall population of solution strings "evolves" toward an optimum solution. The traditional flowchart of genetic algorithms is shown in fig. 1.3.

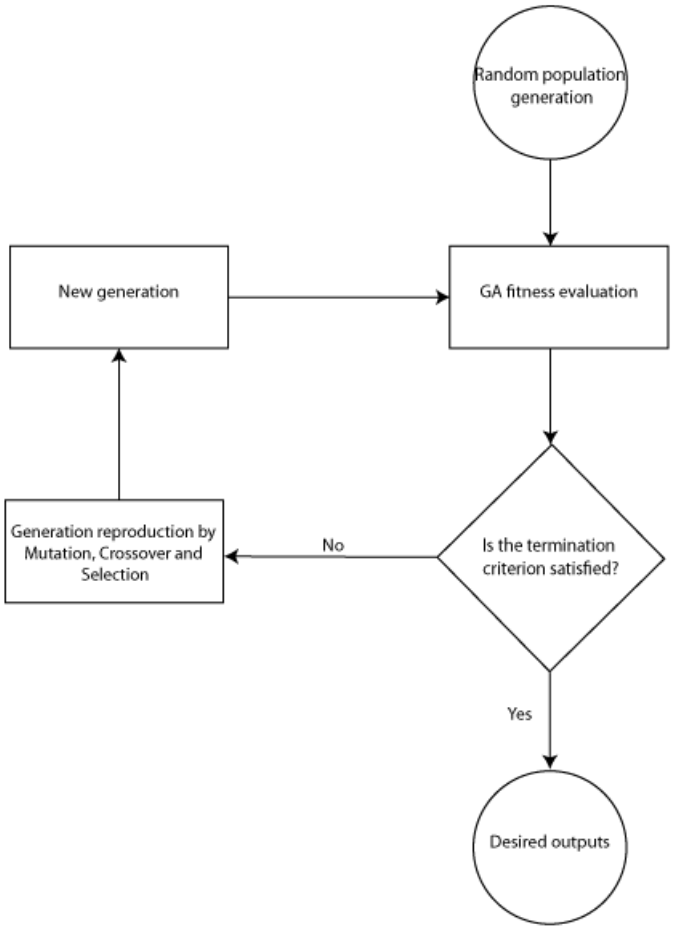

Figure 1.3. The traditional flowchart of genetic algorithm is shown.

Initialization is the selection of the initial population. This can be accomplished either through random selection or seeding a range for which the optimum solution is likely to be

found. For this work, in order to accelerate the process on a single desktop computer, seeds were given where any rational solution might be determined, as will be discussed subsequently.

Genetic algorithms have never been used in the approach described in this thesis. In this approach, the genetic algorithm has been asked to seek solutions to an equation presumed by the user based upon physical mechanisms likely to be operating such that absolute difference between the predicted output (yield strength) and experimentally measured value is minimized. An example of an equation that may be presumed for yield strength, incorporating a generalized form including several types of potential strengthening mechanisms, is shown in equation 1.4.

$$\sigma_{ys} = \sigma_o + \sigma_{ss} + \sigma_{ppt} + \sigma_{disp} + \sigma_{grainsize} + \sigma_{interface} + \ldots \qquad \textbf{Eq. 1.4}$$

where σ_O is the intrinsic flow strength of the material without any other contribution to strength, σ_{SS} is the contribution from solid solution strengthening, σ_{ppt} is the contribution from precipitate strengthening, σ_{disp} is the contribution from dispersion strengthening, $\sigma_{grainsize}$ is the contribution from grain size effects (i.e., the Hall-Petch effect), $\sigma_{interface}$ is the contribution from interfacial strengthening. While other strengthening mechanisms, such as forest hardening, are not included in the example equation above, the modification of the equation is self-apparent.

Each of these individual components may be quite complex. For example, the legacy expression for solid solution strengthening is not only complex, exhibiting potential synergistic effects, but also contains many weighting pre-factors which are unknown. Further complicating some of these individual components is that there are divergent thoughts regarding the form of the equation. Considering solid solution strengthening of an individual alloying addition, for which the equation is often generalized to the form shown in equation 1.5.

$$\sigma_{ss} = Ac^n, n \text{ is } \tfrac{1}{2} \text{ or } \tfrac{2}{3} \qquad \textbf{Eq. 1.5}$$

Interestingly, the precise form of *n*, *which is a fitting parameter*, is either taken as *1/2* or *2/3* depending upon the source. The precise equation to be optimized is presented in the Results and Discussion chapter, along with justifications for postulating its form.

Once the equation has been optimized, genetic algorithms provide two opportunities for feedback. The first is that the weighting pre-factors can take values close to zero. For such cases, it is reasonable to conclude that the contribution of these mechanisms or input variable to the physical property, here the strength of the material, is negligible compared to the attending strengthening mechanisms –thus, indicating as incorrect or minimal presumption. The second is that it is possible to exercise the optimized equation in a manner equivalent as artificial neural networks [3, 13, 20] such that the virtual dependencies of the two equations (the artificial neural network summation of complex hyperbolic tangents and the genetic algorithm optimized phenomenological equation) can be compared. It is expected that this latter feedback will help to identify if an individual input variable has not been properly included (e.g., the form is incorrect) in the phenomenological equation.

It is acknowledged that there may be more elegant methods to compare the two equations (e.g., a minimization of the virtual experiments of both equations). However, this is beyond the scope of this thesis and is left open to wider mathematical community.

Genetic algorithms are tools that can assist in the determination of the optimum yet unknown variables of the expressions for the various phenomenological components (e.g., their prefactors and exponential). Rather than using this approach to search for new alloys, it is proposed in this thesis to use the genetic algorithm to search for the unknown material parameters that are associated with complex phenomenological equations. Using this approach,

it is possible to postulate a phenomenological equation that satisfies all data associated with a given dataset.

Experiments or methods based upon a Monte Carlo approach incorporate random events to calculate a probabilistic solution (or outcome) to a problem (or complex event). Most commonly, these approaches are exploited when the determination of an exact solution in closed-form is not likely, principally when the problem cannot be described in a deterministic manner [21]. Monte Carlo simulations are used widely for a variety of materials science problems where the cascading uncertainties of each successive step make an exact solution highly unlikely, including, for example, cascades in nuclear physics, ion bombardment [22] predictions of microstructure or microstructural evolution, electron microscopy simulations, and studies related to surfaces or grain growth [23-26]. This study seeks to incorporate Monte Carlo strategies to understand how probable it is that a given equation is accurate (for a given database) given these precepts: (1) the phenomenological determination of a single, constitutive equation in multi-component, multi-phase materials is exceedingly difficult given the complexity of the problem; (2) both legacy and current state-of-the-art phenomenological approaches are based upon average microstructural and compositional inputs; (3) equations that are easily expressed are intrinsically deterministic and often fail to capture uncertainties; (4) experimental data contained within the databases are currently expressed as averages; and (5) associated with these averages are uncertainties (e.g., standard deviations from multiple measurements) which are not typically captured in predictive tools. Importantly, this provides a means to "referee" whether the results of the deterministic equation optimized using the genetic algorithm will produce a range of data, given the microstructural uncertainty, that is approximately equivalent to the error as predicted using the neural network. In other words, this determines whether the potential errors of both the

neural network and the genetic algorithm inspired phenomenological equation are nominally equivalent. Monte Carlo method was used to study the effect of uncertainty of data points on the yield value.

This study presents a novel and as-yet unpublished approach by which the power of an artificial neural network (relating inputs to outputs through a complex hidden layer) can be harnessed, and deconstructed into a form that appears to capture the physics according to our legacy understanding. The deconstruction is a framework in which the artificial neural network passes information to genetic algorithms, which minimizes the difference between a postulated equation containing potential operating mechanisms and the complex hyperbolic tangent function. In addition, this thesis shows the importance of incorporating uncertainty of the input data into the model. This last point is important as the Bayesian neural networks automatically incorporates uncertainty through a Gaussian approach to the input data and a strategy incorporating Occam's razor.

CHAPTER 2

LITERATURE REVIEW

In this chapter computational methods including neural networks, genetic algorithms and the Monte Carlo method are explained in detail. Virtual experiments using expressions extracted from well-trained neural networks and genetic algorithms are introduced. The integrated approach principally developed in this thesis to derive a phenomenological equation from a dataset is described. As this thesis seeks to apply this approach to a complex industrially relevant titanium alloy, fundamentals of titanium metallurgy are briefly reviewed - specifically its microstructural evolution and known structure-property relationships. Lastly, as an equation of yield strength must be postulated, some elements of strengthening mechanisms are reviewed.

2.1 Computational Method Review

2.1.1 Neural Networks

Regression models are frequently used to determine the output as a function of input(s). Regression models can be categorized as linear and non-linear regression models. The general form of linear regression models is shown in equation 2.1.

$$y = \sum_{i=1}^{n} a_i x_i + b_i \qquad \textbf{Eq. 2.1}$$

where n is the number of variables, x is the input value, y is the output value and a and b are best-fit parameter values of the slope and intercept, respectively. Some intrinsic limitations reduce the usefulness of linear regression models including 1) the limited flexibility of the model to describe complex functions and 2) inability to capture some types of variables; e.g., Boolean variables. In contrast, non-linear regression models are more flexible. The general form of these models is represented in equation 2.2.

$$y = f(a_i, x_i) + b \qquad \textbf{Eq. 2.2}$$

where y is the output, x is the input, i represents each variable, and f is a more complex function used for the non-linear regression model and a and b are the best-fit parameters. Generally speaking, in comparison with linear regression models these models better capture the real, complex, non-linear relationships that exist among real data for most datasets. However, the usefulness of non-linear regression models is also limited due to intrinsic attributes such as: its inability to capture different kinds of variables; and the fact that the modeling function should be known prior to use. For non-linear regression, the mathematical relation between the inputs (or variables) and the output should be known. Due to these limitations, for the determination of unknown interrelationships from complex databases remains a challenge.

Neural networks are very flexible, non-linear regression models which may be used to model complex databases. It has attributes that are highly desirable when compared with the regression models described previously. For instance, it may be applied to a database without knowing the mathematical relation between the input variables and the output. The schematic of this model is shown in fig. 2.1. This schematic illustrates the different parts of a neural network model. Each neural network model contains three different kinds of layers, namely the input layer, hidden layer(s) and output layer. Moreover, each layer contains one or more neurons. The number of neurons in the input layer represents that number of interrogated variables in the database. For instance, the composition of an alloy may be expressed as discrete (or, perhaps, coupled if relevant) variables of a database. The number of hidden layers and the number of neurons determine the complexity of the model. The number of neuron(s) in the output layer represents the predicted result(s) of the model based on the inputs. For the purpose of this thesis, the output has only one neuron (e.g., yield strength).

The architecture of the hidden layer plays a key role on the performance of the neural networks. In fig. 2.2, the same database was applied to two different architectures. Both architectures have only one hidden layer but they have two different numbers of neurons; i.e., one neuron and six neurons. For the first architecture, the trained model was not able to predict the output properly due to a restricted flexibility for the database. However, for the second architecture, the neural network model is flexible enough to fit itself to the valid model and predict the outputs within ±3% errors.

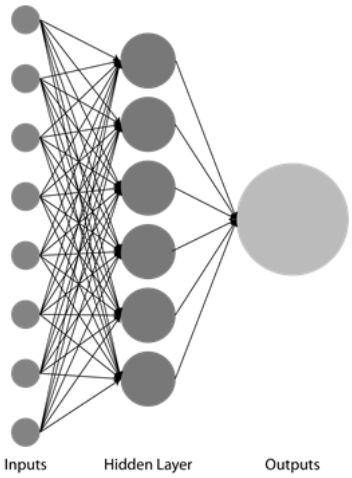

Figure 2.1. A general schematic of a neural network architecture.

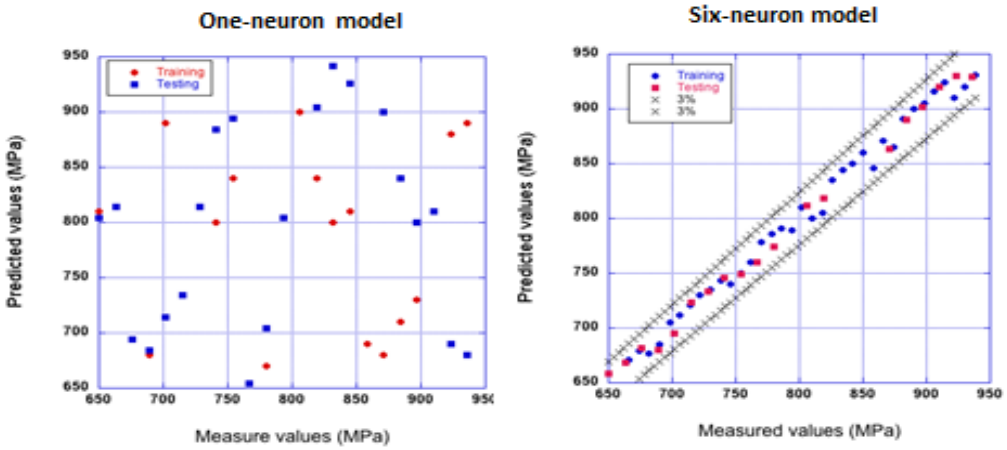

Figure 2.2. The performance of neural networks is highly dependent on its architecture.

Layers are connected to each other by transfer functions. The input layer and the hidden layer are connected by equation 2.3.

$$h_i = f(\sum_j w_{ij}^1 x_j + \theta_i^1) \qquad \textbf{Eq. 2.3}$$

where y is the output, x_j is the input, i is the number of hidden units, w_{ij} is the weight and θ is the bias and f is the transfer function. The output layer and the hidden layer are connected by equation 2.4 where w_i is the weight and θ is the bias and h_i is the value calculated by equation 2.3. An iterative process to optimize weights and biases is applied to fit the model. The degree of non-linearity of a model is determined by the type and the number of transfer functions used in the model.

$$y = \sum_i w_i^2 h_i + \theta^2 \qquad \textbf{Eq. 2.4}$$

A one-hidden-layer Bayesian neural network was used in this thesis. The transfer function which connects the input layer to the hidden layer is shown in equation 2.5. The transfer function which connects the hidden layer to the output layer is the same as equation 2.4.

$$h_i = \tanh(\sum_j w_{ij}^1 x_j + \theta_i^1) \qquad \textbf{Eq. 2.5}$$

Since the hyperbolic tangent function is a very flexible function, it is frequently used in the neural network modeling. This function is able to fit itself to very complex relationships that might be present in a database. To validate the architecture, the database is typically divided into two sets; the training dataset and the testing datasets. Normally, the training dataset contains ~2/3 of the database and its members are selected randomly. It is worth noting that the inputs containing the extreme values should be included in the training dataset to get the best result. To give an equivalent chance to all the variables to contribute to the model, all inputs and output are normalized between -0.5 and 0.5 according to equation 2.6.

$$x_N = \frac{x - x_{\min}}{x_{\max} - x_{\min}} - 0.5 \qquad \textbf{Eq. 2.6}$$

where x_N is the normalized value, x is the measured value, x_{min} and x_{max} are the minimum and maximum values of all the inputs in each variable, respectively. For the training dataset, both the inputs and the output are introduced to the neural network model. Conversely for the testing dataset, only the inputs are introduced and the model seeks to predict the output. The model is evaluated and the weights and biases are gradually optimized in successive iterations by the outputs of the testing dataset. It should be noted that the initial weights and biases are randomly selected. To optimize the weights and biases, the objective function, $M_{(w)}$, (equation 2.7) should be minimized.

$$M_{(w)} = \beta E_D + \sum_c \alpha_c E_{w(c)} \qquad \textbf{Eq. 2.7}$$

where E_D is the error function (equation 2.8), $E_{w(c)}$ is the regularizer term (equation 2.9), α_c and β are the controlling parameters shown in equations 2.8 and 2.9, respectively. The error function is given by:

$$E_D(w) = \frac{1}{2}\sum_m (y_p - y_m)^2 \qquad \textbf{Eq. 2.8}$$

where y_p is the predicted value by the model and y_m is the measured value for that input in the testing dataset. The regularizer term is given by:

$$E_{w(c)} = \frac{1}{2}\sum_{i \in c} w_i^2 \qquad \textbf{Eq. 2.9}$$

where c shows each class of weights. For instance, the weight class which connects the input layer to the hidden layer and w is a weight value. The noise level σ_v is given by:

$$\sigma_v^2 = \frac{1}{B} \qquad \textbf{Eq. 2.10}$$

and the weight variance $\sigma_{w(c)}$ of the model is given by:

$$\sigma_{w(c)}^2 = \frac{1}{\alpha_c} \qquad \textbf{Eq. 2.11}$$

Based on the weight variance values, there will be an error bar for each predicted output by the Bayesian neural network model. The error bar indicates the degree of uncertainty in the fitting parameter. Sometimes to get more accurate predictions, the average of predicted values by selected "best models" is considered as the predicted "output" value. This type of model is called a committee model.

While a flexible modeling approach, the neural network method has characteristics which limit its applicability. The first is the inability to extrapolate to values beyond the database. The extremely flexible hyperbolic tangent function is particularly problematic. Consider the simple example of comparing the results of $y_1=2*x$ and $y_2=2*x+(x-1)*(x-2)*(x-3)*x^3$ over the training range; an integer value between one and three. For the training data, both are equally valid. However, beyond the range the two equations y_1 and y_2 give remarkably different values. This example is shown in Table 2.1.

Table 2.1. Different values for y_1 and y_2

x	y_1	y_2
1	2	2
2	4	4
3	6	6
4	8	392

The second is the difficulty associated with determining the optimum architecture. As shown in fig. 2.2, an increase in the number of neurons improves the fitting parameter of the model and enables the model to predict the results within ±3% error. However, an overly

complex model may "over-fit" the equation to the data. In this case, the model is highly fitted to the training database, but it is well fitted to the full database. As a result, the performance of the model in predicting the outputs of the testing results is poor.

2.1.2 Virtual Experiment by Neural Networks

Once the neural network model has been developed and an equation extracted, it can be exercised to conduct virtual experiments in order to understand the influence of the individual input variables on the resulting output. As noted, it is highly doubtful that these experiments could be conducted in the laboratory due to the interdependence of the various compositional and microstructural variables. In virtual experiments, a database is created in which all variables, except one, have fixed values. Only one variable changes from the minimum value to its maximum values. It should be noted that the absolute values of virtual experiments may not be reliable; however, the given trend is likely reasonable. An example of the type of clarity that can be observed is shown in fig. 2.3, which shows the raw data for thickness of the alpha laths and its influence on yield strength of the raw data (fig. 2.3(a)) and the virtual experiment (fig. 2.3(b)).

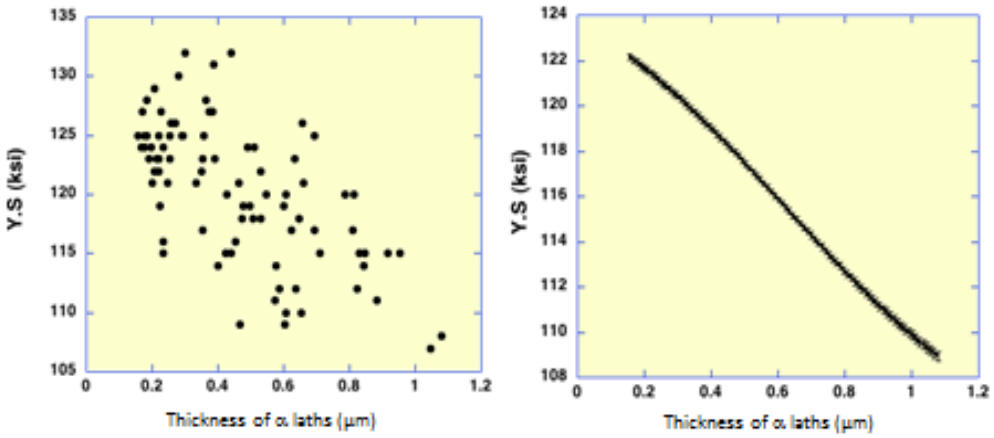

Figure 2.3. No results can be concluded from raw data while from the virtual experiments it can be said that the yield strength id inversely proportional to the lath thickness, after Kar et.al. [3].

2.1.3 Genetic Algorithm

A typical way to determine optimum values of a function is to evolve the function until their "roots" are at optimum values. The normal method of finding extrema is determining the derivative of the principal function and finding the roots of that derivation. However, there are some functions for which the derivative is not solvable. For instance, classical optimization methods cannot find the global minimum and maximum of discontinues functions. Another example function is shown in fig. 2.4. The global minimum of this function is hidden by several local minima.

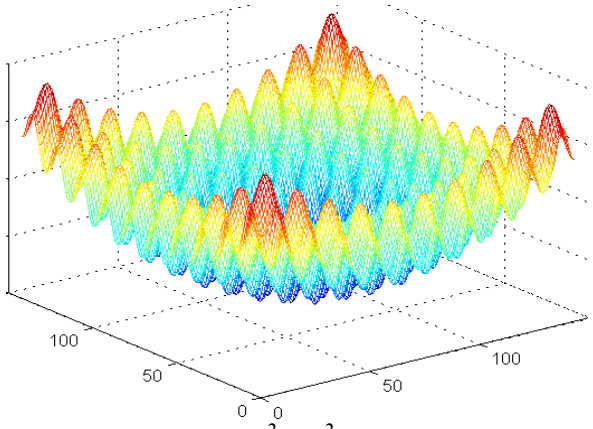

Figure 2.4. The equation is $y=20+x_1^2+x_2^2-10(cos2\pi x_1+ cos2\pi x_2)$ [27].

A genetic algorithm is an optimization method that may be used to find the global minimum or maximum of non-differentiable functions (or any function for which classical methods of optimization cannot be applied). This optimization method imitates natural selection processes in biological evolution. In genetic algorithms, a pool of possible answers (population) is defined. The global minimum or maximum, which is one member of the pool, based on some "randomly-based" well-bounded rules, evolves during several iterations while other possible answers do not. The objective function is called the fitness function. An individual of the population is a vector containing the values of all the variables of the fitness function. This

multi-variable vector is equivalent to a biological “genome” for which each member of the vector is a gene. A score is the value of the fitness function if the genes are the inputs to the multivariable “genome”. The population is a series of individuals used to determine the global minimum or maximum values; i.e. roots, of the fitness function. To achieve the optimum result, it is important to define the population in a way that all possible answers are included. In this case the individuals should be diversely distributed in the pool.

There are three ways to generate children from their parents:

1- By random change to the parents, it is possible to create children. This method is called mutation.

2- By summation of a pair of parent vectors which are selected randomly. This method is called crossover.

3- Some parents have the smallest fitness function values. They are survived during the evolution. This method of keeping some parents to the next generation is called elite.

The schematic of these three methods is shown in fig. 2.5.

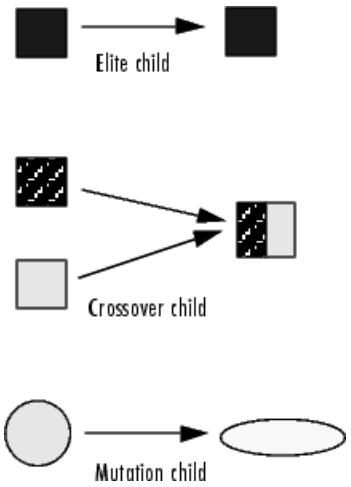

Figure 2.5. All the reproduction methods are shown [27].

The way that these three rules evolve the population is shown in fig. 2.6. In this figure, the reproduction of a new generation from their parents is shown. For the first iteration, from the dark blue parent, some new children -- green, blue and yellow circles -- can be created. By

looking at fig. 2.6-b, it is easily understood that the yellow child is in a direction which advances towards a local maximum. Therefore the yellow circle is not allowed to reproduce a new child. The blue and green circles, or arrows in fig. 2.6-b, have higher fitness values and they survive the 1st generation and reproduce new children. In the second generation, the blue circle is repeated. It shows that the fitness value of the blue circle was very high and the genetic algorithm decided to keep it as the next generation. This reproduction method is called elite. The second method of reproduction is mutation. From a parent which qualified to reproduce a new generation, a new child is created by randomly selecting a value close to the value of the parent. This method of reproduction which is shown by green and purple circles (fig. 2.6(a)), or arrows (fig. 2.6(b)), is called mutation. The third method of reproduction is crossover. In this method, a new child is created by the summation of two qualified parents. The green and blue circles in the 1st generation create the dark blue child in the 2nd generation.

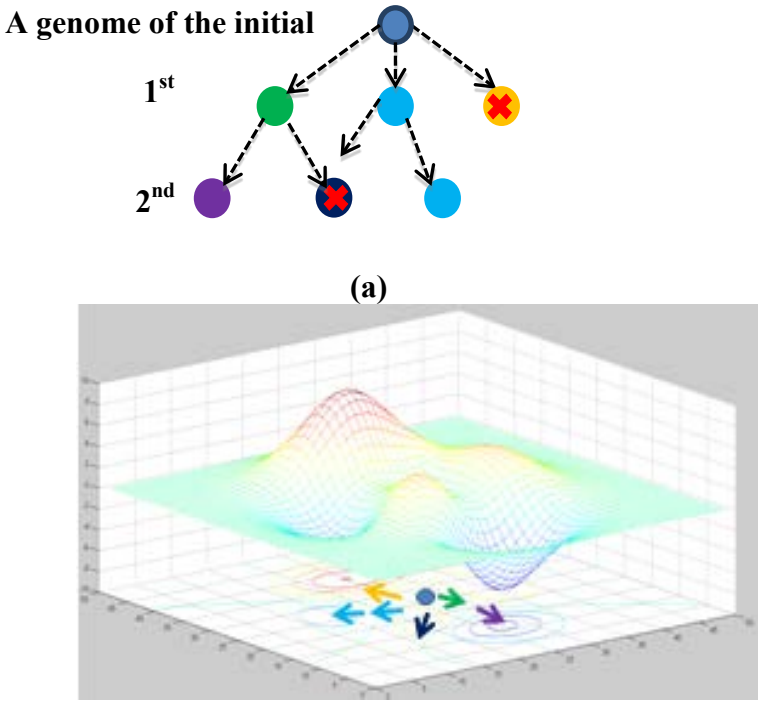

(a)

Figure 2.6. (a) A population evolution is shown. (b) The reproduction map represented in (a) is displayed.

The initial population of genes for the genetic algorithm is random, where the envelope for each genome can be defined either broadly or narrowly by the programmer. Based on fitness function values for each individual, the individuals are ranked. Some of the individuals which have smaller fitness function values are selected as parents to generate the next generation. The next generation is created by three rules; i.e., elite, mutation and crossover. The genetic algorithm flowchart is shown in fig. 2.7.

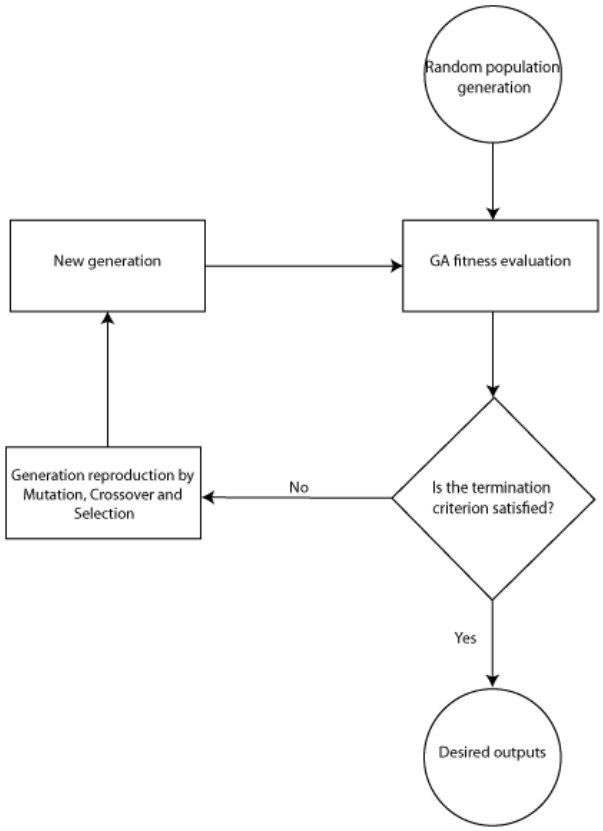

Figure 2.7. A flowchart of the genetic algorithm process is demonstrated.

2.1.4 Virtual Experiment by Genetic Algorithm

Similar to section 2.1.2, it is possible to conduct virtual experiments for the phenomenological equation derived by the genetic algorithm. Here, the same database that was used in the neural network is used. The results of the virtual experiments show the functional

dependency of the postulated equation that was optimized using the genetic algorithm approach. By comparing these virtual experiments with those obtained using neural networks, it is possible to assess the accuracy of the equations and to determine whether any discrepancies between the results.

2.1.5 Monte Carlo

The Monte Carlo method is a computational method based upon the ability to successfully conduct a series of calculations with stochastic variations in certain parameters. It is used in problems with many degrees of freedom in which the calculation of the exact value of the result is virtually impossible. In this method, first all possibilities for the stochastic variations are determined. Then they are randomly selected and the combination effect of those possibilities on the final result is studied. By increasing the number of calculations, it is possible to determine all the possibilities.

2.2 Review of Titanium Metallurgy

2.2.1 Microstructural Evolution

Pure titanium has two allotropic forms - the α and β phases. The alpha phase is hexagonal close packed (hcp) and the beta phase is body centered cubic (bcc). In Ti alloys, elements such as Al and O stabilize the alpha phase and other elements such as V and Fe stabilize the beta phase. The beta phase is stable above the beta-transus temperature (a temperature at which β transforms to α, and is approximately 975°C for Ti-6-4). By definition, beta stabilizers reduce the beta-transus temperature and alpha stabilizers increase the β-transus temperature. Depending upon the thermomechanical processing condition, different

microstructures with significantly different mechanical properties can be achieved.

The first common microstructure is the β processed microstructure. This microstructure is achieved by conducting thermomechanical processing at temperatures above the beta-transus temperature. The microstructure contains Widmanstätten lath-like precipitates of the alpha phase distributed in the beta phase. Fast cooling results in basketweave microstructure while slower cooling rates give colony microstructure in which alpha-lath and beta-rib are geometrically parallel. In both of these microstructures, the Burgers orientation relationship, given below, is almost always satisfied.

$$(110)_\beta \parallel (0001)_\alpha$$

$$[111]_\beta \parallel [1120]_\alpha$$

The colony and basketweave microstructures are shown in fig. 2.8 and 2.9, respectively.

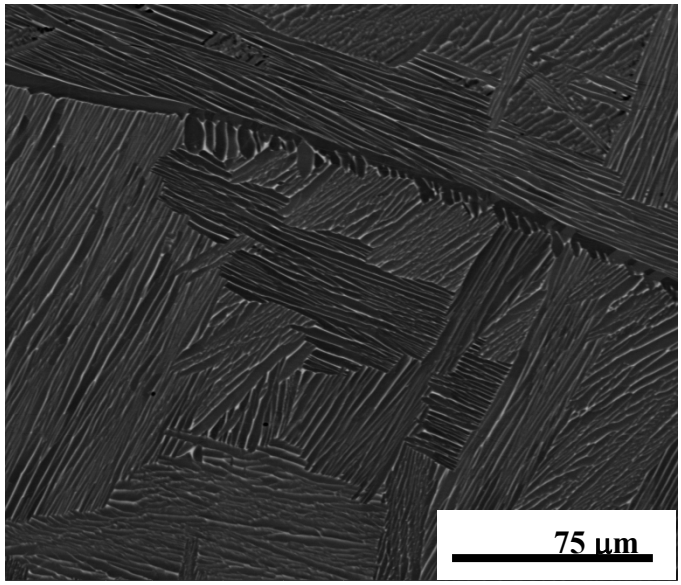

Figure 2.8. Colony microstructure is shown.

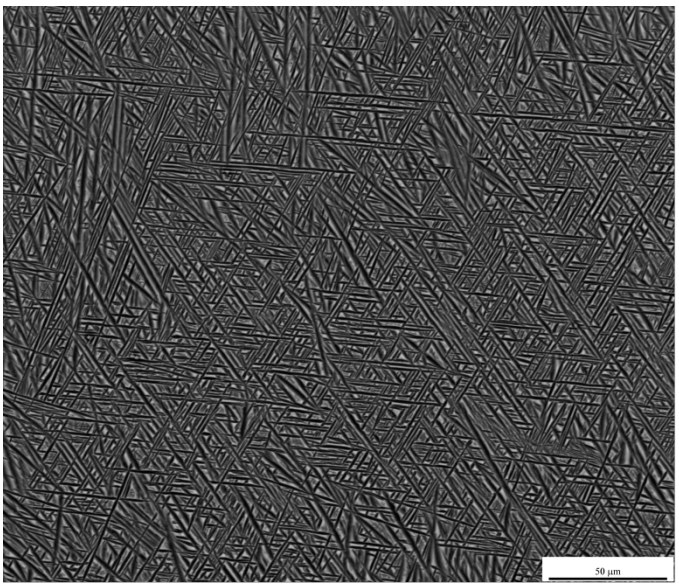

Figure 2.9. Basketweave microstructure is shown.

The second microstructure is the α+β processed microstructure. This microstructure is achieved by conducting thermomechanical processing at temperatures below the beta-transus temperature. The microstructure contains equiaxed alpha particles in addition to the transformed β microstructure. An example of this microstructure is shown in fig. 2.10. Equiaxed alpha particles do not obey the Burgers orientation relationship.

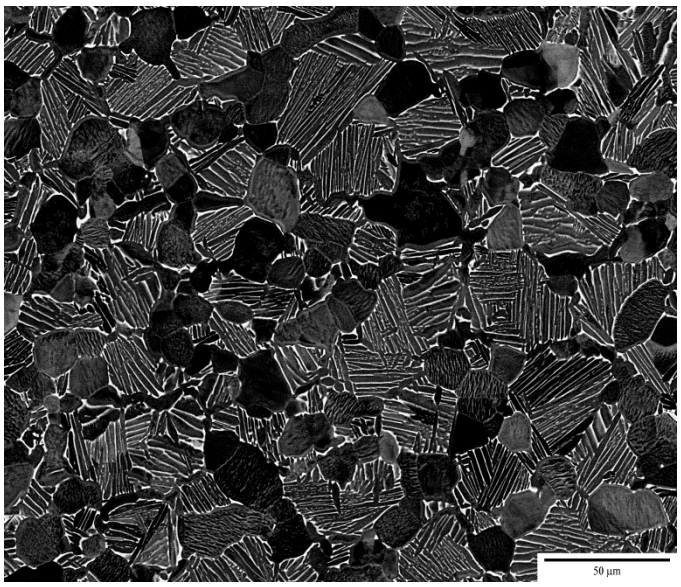

(a)

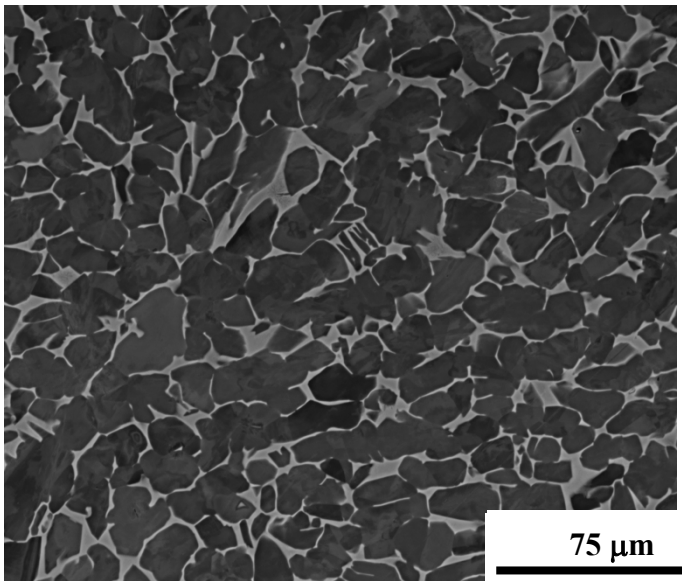

Figure 2.10. (a) A typical α/β processed microstructure is shown. This microstructure contains both colony and equiaxed microstructure. (b) A well-developed equiaxed alpha microstructure in the beta-phase matrix is presented.

2.2.2 Mechanical Property Relationships

Deformation in titanium alloys can be categorized as glide and twinning. <a> type dislocations are mobile on the prismatic planes and <c+a> type dislocations are also mobile on the pyramidal planes. Twining has often been observed when the deformation happens at low temperature or high strain rate.

The mechanical properties in titanium alloys are highly dependent on the composition and the microstructure. For instance, α/β processed titanium alloys consisting of a bimodal microstructure are used in low cycle fatigue applications [28] while β processed alloys are characterized by improved high cycle fatigue strength [29]. It is believed that colony microstructure has lower ductility than equiaxed alpha particles [30]. The reason is that in the colony microstructure it has been suggested that only basal system is activated for glide while in equiaxed alpha microstructure more slip systems are activated.

Researchers proposed different microstructural features which are affecting mechanical properties in titanium alloys. For example, the α colony size has the highest contribution to the mechanical properties in the β processed alloys due to the relation between the size of the α colony and the effective slip length [1]. For α/β processed alloys, it has been suggested that the volume fraction of primary (equiaxed) alpha and prior beta grain size plays a key role in mechanical properties [31].

2.2.3 Basics of Strengthening Mechanism

Strengthening mechanisms in metallic materials can occur when plastic deformation due to dislocation glide, twinning or phase transformation is disrupted [32]. Some important strengthening mechanisms are:

1. Solid-solution strengthening
2. Age/precipitation hardening
3. Dispersion strengthening
4. Grain size reduction
5. Strengthening from cold work
6. Strengthening from the interface

Interestingly, many of the above mechanisms are themselves somewhat interrelated. This often complicates the isolation of additive effects of mechanisms on yield strength. For example, precipitation hardening has as an embedded influence interfacial/chemical strengthening. Regarding Ti-based alloys, and their complex microstructures, the strengthening mechanisms are unknown. However, based upon the previous neural network modeling of α+β processed Ti

[13], the strengthening mechanisms are likely to include solid solution strengthening, size effects, and strengthening from interfaces. These are described briefly.

2.2.3.1 Solid Solution Strengthening

Solid solution strengthening is the result of dislocation interaction with solute atoms. The are two possible reasons for solid solution strengthening 1) elastic modulus difference between the solute and solvent atoms 2) interaction of the strain field of dislocations with those of solute atoms. This interaction can be attractive or repulsive. If the interaction is attractive, the energy of the dislocations reduces and they are locked by the solutes. Therefore, more shear stress needed for dislocation motion and the material is strengthened. If the interaction is repulsive, the energy of the dislocations increases when they are close to solute atoms and the dislocation energy increases. The material is strengthened due to an increase in the resolved shear stress needed for dislocation motion.

There are two ways to model solid-solution strengthening:

1. Interaction of a random fixed dispersion of solutes with dislocations: based on this approach, the total solid solution strengthening of two solute elements *A* and *B* is calculated according to equation 2.12 [33, 34].

$$\Delta\tau_{ss}^{total} = (\Delta\tau_A^{2/3} + \Delta\tau_B^{2/3})^{3/2} \qquad \textbf{Eq. 2.12}$$

2. Slip nucleation at a barrier of solute atoms: The model developed based on the work needed for movement of an edge dislocation from one linear segment of pinning solutes to the next one. This model helps us better understand temperature dependency of solid solution strengthening.

2.2.3.2 Size Effects (Analogous to the Hall-Petch Relationship)

According to the Hall-Petch relationship (equation 2.13), the strength of a material increases by reducing the grain size.

$$\sigma_y = \sigma_i + kd^{-0.5} \qquad \textbf{Eq. 2.13}$$

where σ_I is the intrinsic lattice friction stress, k is a material constant and d is the grain size. Yield strength as a function of grain size for different crystal structures is shown in fig. 2.11.

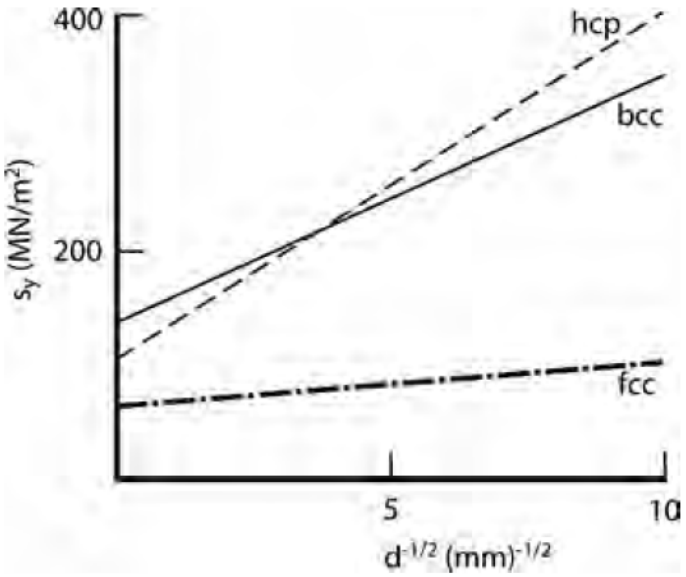

Figure 2.11. The effect of grain size on the yield strength for different crystal structures is shown [32].

In polycrystalline metals, increasing the load initiates slips in grains which have the maximum Schmid factor. The emitted dislocation loops extend up to the time they reach an obstacle (e.g., a grain boundary). Due to the mismatch on both sides of the grain boundary, a dislocation slipping on a slip system on one side cannot go to the other side and it stops at the grain boundary. The next dislocation which is approaching the grain boundary is repelled by the previous dislocation(s) stuck at the grain boundary. Therefore a greater applied load is needed to move the second dislocation with respect to the first dislocation. Due to the accumulation of

dislocations at the grain boundary, a stress pile up forms at the grain boundary which is able to induce dislocations on the other side of the grain boundary. If the grain is large, the number of accumulated dislocations at the grain boundary is large and the stress concentration factor would be considerable. As a result, a small load is enough to activate slip systems in grains with lower Schmid factors. In contrast, in small grains, few dislocations are contributing to the pile up and more load is needed to generate dislocations on the other side of the grain boundary.

2.2.3.3 Interfacial Strengthening

Another mechanism of strengthening is interfacial strengthening which forms in lamellar microstructures containing two phases, e.g. colony microstructure in Ti-6-4. The interphase interface hinders the transmission of electrons from one side of the interface to the other side. This hindrance is inversely proportional to how much parallel the slip planes on both sides of the interface are. Dislocations which pass the interface leave a defect at the interface.

CHAPTER 3

EXPERIMENTAL AND MODELING PROCEDURE

3.1 Experimental Procedure

The database used in this study was developed in a research program at The Ohio State University [13]. Nine compositionally different alloys in the specification range of Ti-6Al-4V alloy (in wt%) were prepared. In these alloys, the composition of four important elements; i.e. Al, V, Fe, and O changed as follows:

Al: 4.76-6.55; V: 3.30-4.45; O: 0.07-0.20; Fe: 0.11-0.41

The composition of each alloy was measured by Timet using the inductive coupled plasma (ICP) method. The composition of all the alloys is tabulated in Table 3.1. To reduce the effect of texturing on the mechanical properties, the samples were cut from the same radius of the billet. Therefore, in this study the effect of texturing on the yield strength was not considered.

Table 3.1. The composition of different samples.

Al	V	Fe	O
4.85	4.45	0.11	0.198
4.76	4.27	0.39	0.072
6.55	4.38	0.407	0.197
6.55	3.38	0.394	0.071
5.64	3.83	0.252	0.135
4.766	3.297	0.11	0.08
6.514	4.29	0.11	0.079
6.495	3.313	0.107	0.19
4.79	3.35	0.39	0.196

To measure the yield strength values, the samples were subjected to mechanical testing at room temperature. As described in the literature regarding the population of this database, four optical and SEM images were taken from metallographic samples excised from the grip region and examined using an FEI FEG Sirion scanning electron microscope (SEM) operating in

backscattered electron imaging mode at 15 kV with a resolution of approximately 3.0 nm. The microstructural features which were quantified are equiaxed α size (μm), the volume fraction of equiaxed α, the volume fraction of total α, and the width of the α-laths in the transformed β regions (α-lath width, μm). The quantification procedure for each microstructural feature is well explained in the literature [35].

3.2 Computational Procedure

Three different computational approaches have been integrated in this work. They are described while concurrently describing the integrated approached adopted in this study. It should be noted that the fundamentals of each method was discussed in chapter 2.

3.2.1 Artificial Neural Networks

For this work, the experimentally determined data regarding alloy composition, microstructure, and tensile properties populated a database for subsequent analysis. The database was separated into two parts, one for training (40 samples), and the other for testing (16 samples). This probabilistic neural network was used to develop a model which predicts the interrelationships between microstructure and properties of α/β processed Ti-6Al-4V. All the samples with extreme values were selected as training samples. Other samples were randomly distributed among the training and testing datasets. The best model architecture was one-hidden layer containing six neurons. 1000 was used as the seed value to generate a set of random numbers which are assigned to the weight parameters as their initial values. The initial width of the Gaussians corresponding to the weight parameters associated with the inputs variables and output was 0.1. Since there was no significant difference between the best model and the

committee model containing the best three models, only the best model was considered as the neural network model. The input layer contained eight neurons which are Al, V, O and Fe concentration in (wt%) and volume fraction total alpha, volume fraction of equiaxed alpha particles, mean equiaxed alpha size and lath thickness. The output layer had only one neuron -- yield strength value. Once developed, the model was exercised to conduct virtual experiments in order to understand the influence of the individual input variables (composition, microstructure) on the resulting properties. To do virtual experiments, all the variables, except one, were fixed to the average value and only one variable changed from its minimum value to its maximum value.

3.2.2 Genetic Algorithms

A genetic algorithm developed in global optimization toolbox of MATLAB 2011 was used to find the global minimum of the proposed function. The number of variables was set to 22. The initial population size was 100. The fitness scaling function was fitscalingrank. The contribution of elite, crossover and mutation in reproduction was 20%, 40% and 40%, respectively. A "while loop" with "maximum error more than *5%* in predicted vs. measured plot" expression was used to get the optimum result from the algorithm.

3.2.3 Monte Carlo

The average of the individual standard deviation values for each off the 54 data points for a given microstructural feature from the experimental database were taken as the uncertainty values for the four microstructural features, namely total volume fraction of alpha phase, mean equiaxed alpha size, volume fraction of equiaxed alpha phase and lath thickness. Different random possibilities were studied in 30 iterations to determine the maximum yield deviation

(MYD) values with respect to the value predicted by the genetic algorithm for each variable while the other variables were held constant at their average values (identical to what is done using neural networks). The difference between the GA and NN results was defined to be zero if a member of GA-predicted value $\pm$ MYD interval is a member of NN-predicted value $\pm$ noise interval. The effect of MYD and noise on the predicted *GA-NN* values can be separately studied by dividing the interval to smaller intervals; i.e., GA-predicted value+MYD, GA-predicted value-MYD, NN-predicted value+noise interval, and NN-predicted value-noise intervals and comparing their values to GA and NN predicted values prior to MC calculations.

3.2.4 Integrated Approach

Initially, the neural network approach was used to derive a model without having knowledge of the physics of the problem. After finding the best neural network architecture, virtual experiments were performed to obtain the functional dependency of each variable, noted as "A" in fig. 3.2. Then the genetic algorithm was used to assess various postulated yield strength equations with unknown fitting parameters to a phenomenological model. First, a possible phenomenological equation, to calculate yield strength values (MPa) as a function of the composition and microstructure, with unknown precursors and powers were proposed. The unknowns were determined by minimizing the difference between values predicted by the proposed equation and the measured values. In a manner similar to the trained neural network model, virtual experiments were then performed using the same database by the optimized equation (labeled as "B" in fig. 3.2). The virtual experiment results calculated by the proposed equation were compared to the neural network virtual experiment results. The comparison gave the chance to correct the proposed equation, adding or dropping term to the equation (e.g., when

a pre-factor was identified as 0). Finally, the Monte Carlo method was used to study the effect of uncertainties in the measurements, e.g. lath thickness size, on the output. The complete scheme of the integrated approach is shown in fig. 3.1.

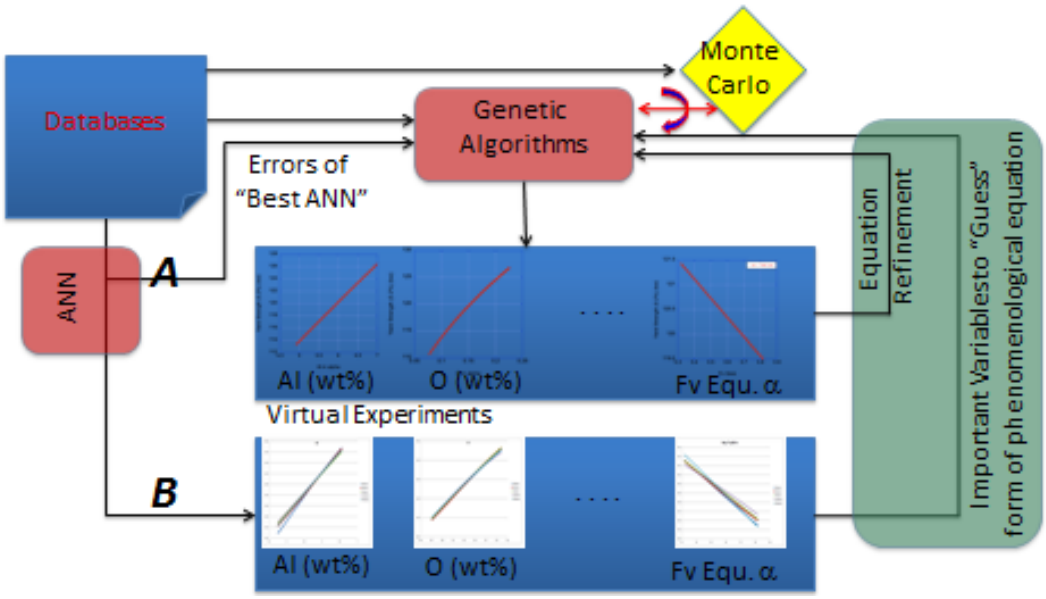

Figure 3.1. The integration of neural networks, genetic algorithm and Monte Carlo is shown.

CHAPTER 4

RESULTS AND DISCUSSIONS

4.1 The Equation

Equation 4.1 has been proposed based on virtual experiments performed by the neural network shown in fig.4.1(a-d) and fig.4.2(a-d), which are nominally identical to the previously published results, and by considering well-developed legacy strengthening expressions.

$$\sigma_{ys}(MPa) = (\sigma_0^{\alpha} * F_V^{\alpha}) + (\sigma_0^{\beta} * F_V^{\beta}) + F_V^{\alpha} * (A_{Al} * C_{Al}^{n_{Al}} + A_O * C_O^{n_O}) +$$
$$F_V^{\beta} * ((A_V * C_V^{n_V})^{n_1} + (A_{Fe} * C_{Fe}^{n_{Fe}})^{n_2})^{n_3} + F_V^{equiaxed\_\alpha} * k_y * Equiaxedsize^{-n4} +$$
$$(1 - F_V^{equiaxed\_\alpha}) * (C + B * \frac{\frac{size\_equiaxed\_\alpha}{F_V^{equiaxed\_\alpha}} - size\_equiaxed\_\alpha}{Lathwidth} +$$
$$k_{y'} * (\frac{Equiaxedsize}{Fvequiaxed} - Equiaxedsize)^{-n5}) +$$
$$B'' * \frac{(F_V^{\alpha} - F_V^{equiaxed\_\alpha}) * Lathwidth - MINLath}{MAXLath - MINLath} * F_V^{\beta} + B''''(Lathwidth)^{-n6}$$

Eq. 4.1

(a)

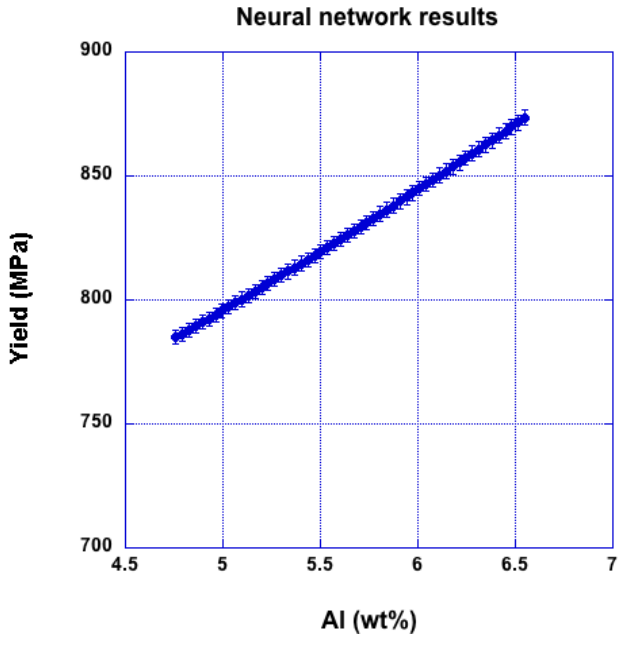

(b)

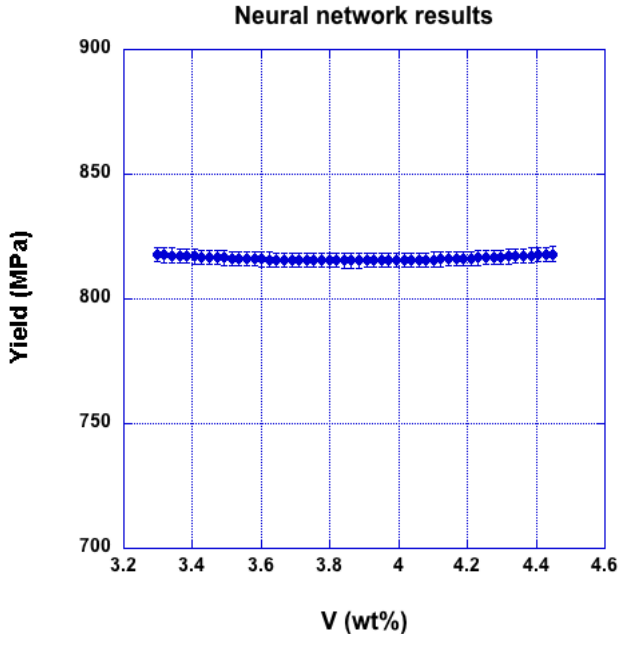

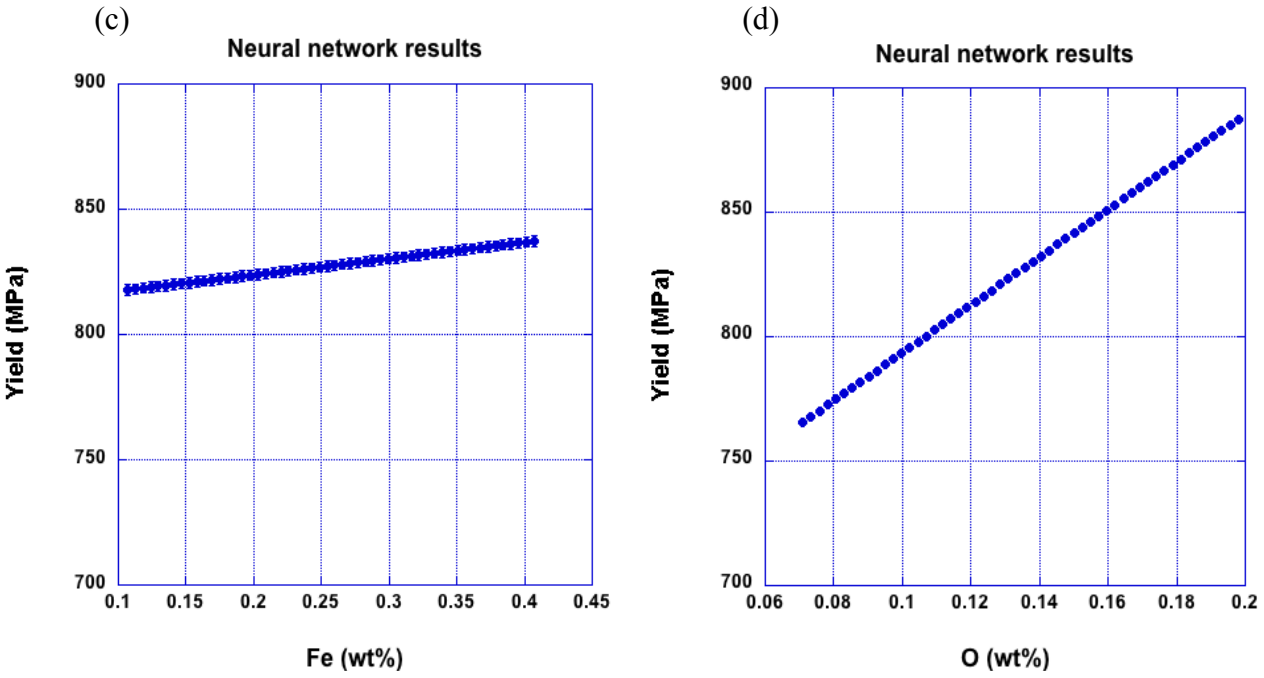

Figure 4.1. The effect of (a) Al, (b) V, (c) Fe and (d) O (wt%) on the yield strength was studied by virtual experiments conducted by neural networks.

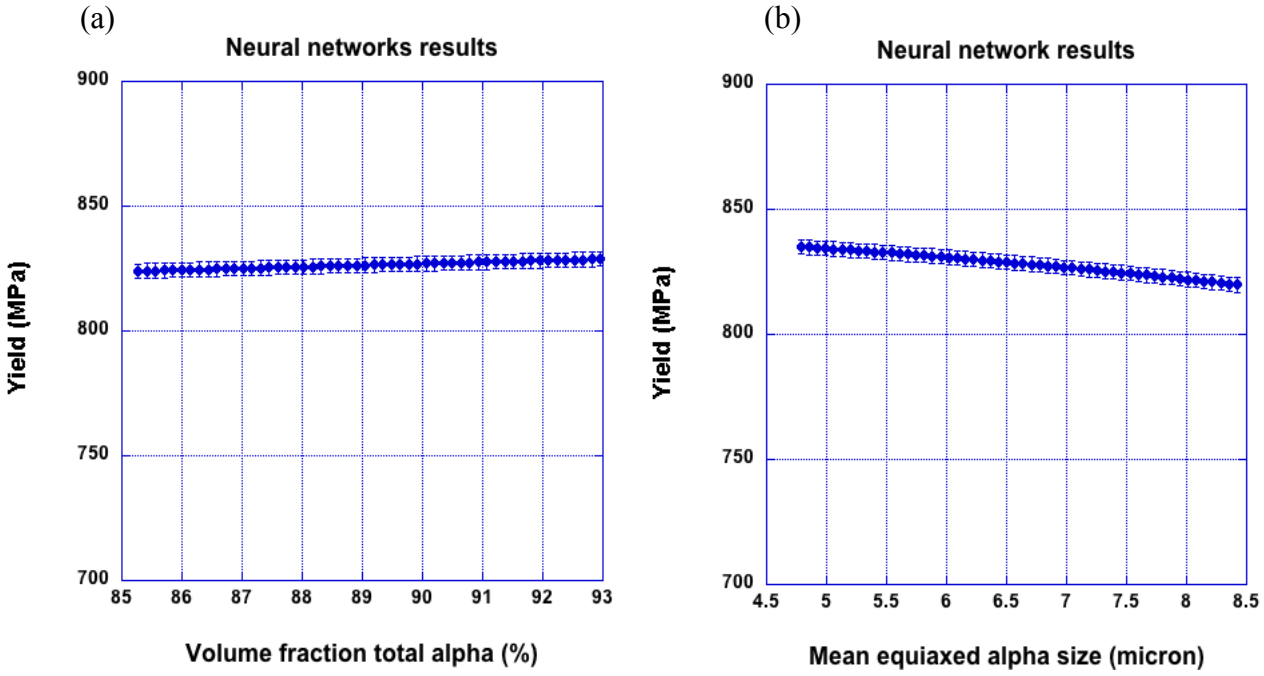

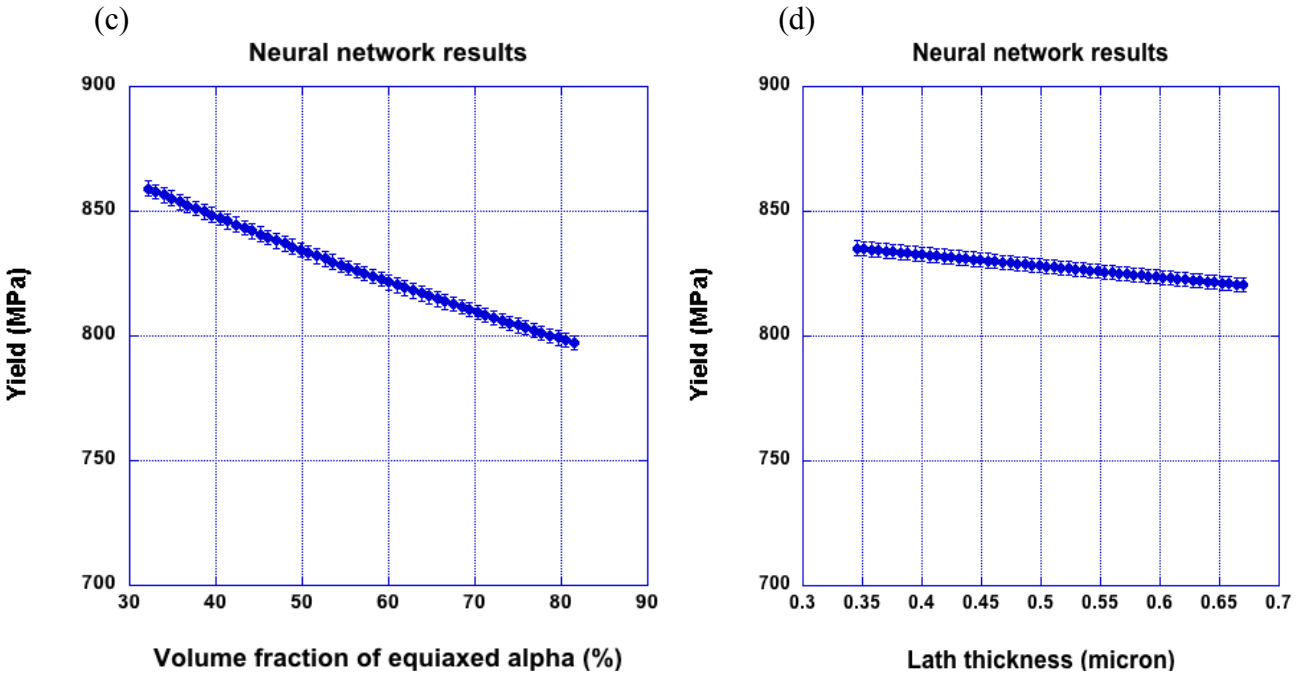

Figure 4.2. The effect of (a) volume fraction total alpha (%), (b) mean equiaxed alpha size (μm), (c) volume fraction of equiaxed alpha (%) and (d) lath thickness (μm) on the yield strength was studied by virtual experiments conducted by neural networks.

The 22 unknown variables in equation 4.1 are intrinsic flow strength of alpha and beta phases (σ_0^{α} and σ_0^{β}), solid solution strengthening precursors (A_{Al}, A_O, A_{Fe}, A_V) and exponents (n_{Al}, n_O, n_{Fe}, n_V),synergistic effect (n_1,n_2,n_3), Hall-Petch strengthening in equiaxed alpha particles (k_y), strengthening in the transformed beta phase (C), the interfacial strengthening effect (B), Hall-Petch strengthening in colonies of parallel alpha laths (ky'), the effect of constrained beta (B'') and Hall-Petch strengthening for lath width (B'''').

Since the postulated equation 4.1 has 22 unknown variables, it is too difficult to extract the equation without knowing any value for the variables. The novel method proposed in this thesis paves the way to determine the equation. Initially, neural networks are using to capture a mathematical model which fits the database. Then, the genetic-algorithm-derived phenomenological equation is solved and modified by comparing the results of genetic algorithm

with the neural network results. To evaluate the validity of the phenomenological equation, the virtual experiments performed by genetic algorithm and neural networks were compared. Genetic algorithm virtual experiments are shown in fig. 4.3 and 4.4; they are considerably in good agreement. The optimized form of equation 4.1 is shown in equation 4.2. Below, each term that contributes to equation 4.2 is discussed.

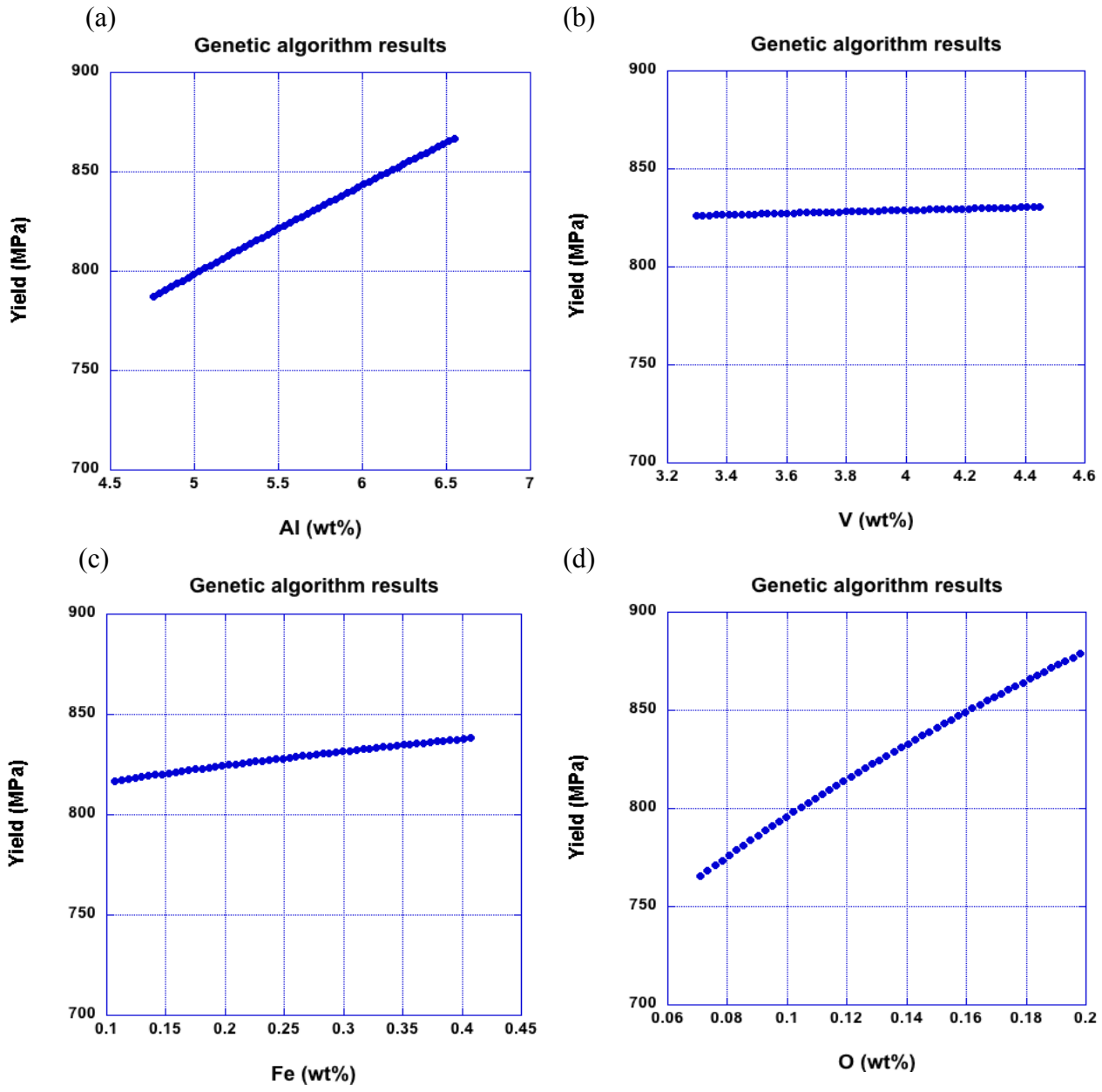

Figure 4.3. The effect of (a) Al, (b) V, (c) Fe and (d) O (wt%) on the yield strength was studied by virtual experiments conducted by the phenomenological equation.

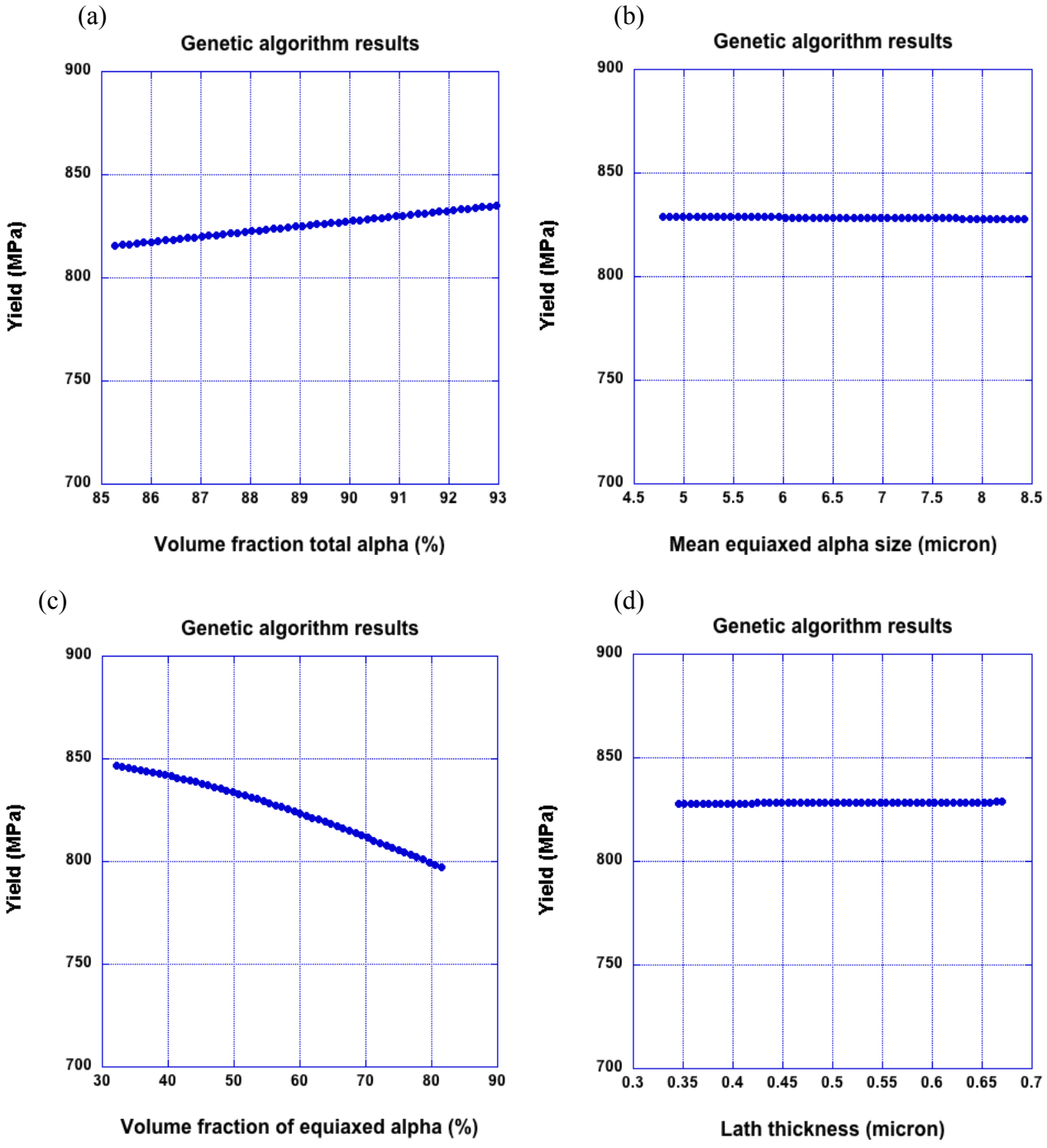

Figure 4.4. The effect of (a) volume fraction total alpha (%), (b) mean equiaxed alpha size (□m), (c) volume fraction of equiaxed alpha (%) and (d) lath thickness (□m) on the yie studied by virtual experiments conducted by the phenomenological equat

$$\sigma_{ys}(MPa) = (88.5 * F_V^{\alpha}) + (63 * F_V^{\beta}) +$$
$$F_V^{\alpha} * (148.5 * C_{Al}{}^{0.63} + 724.5 * C_O{}^{0.6}) +$$
$$F_V^{\beta} * ((49.8 * C_V{}^{0.63})^{0.45} + (240 * C_{Fe}{}^{0.82})^{0.48})^{2.12} +$$
$$0.02 * F_V^{equiaxed\_\alpha} * Equiaxedsize^{-0.33} +$$
$$(1 - F_V^{equiaxed\_\alpha}) * (154 + 0.15 * \frac{\frac{size\_equiaxed\_\alpha}{F_V^{equiaxed\_\alpha}} - size\_equiaxed\_\alpha}{Lathwidth} +$$
$$0.01 * (\frac{Equiaxedsize}{Fvequiaxed} - Equiaxedsize)^{-0.32}) +$$
$$18.5 * \frac{(F_V^{\alpha} - F_V^{equiaxed\_\alpha}) * Lathwidth - MINLath}{MAXLath - MINLath} * F_V^{\beta} +$$
$$0.015 * (Lathwidth)^{-0.53}$$

Eq. 4.2

4.2 Intrinsic Flow Strength

In the literature, different and widely disparate values of yield strength can be found for commercially pure titanium [31-34]. This inconsistency arises due to 1) it is so difficult to make titanium very pure thanks its tendency to getter other elements (i.e., it is the "universal solvant") and 2) variations in trace levels of oxygen and iron, commercially pure titanium is classified to different grades. For example, in grade 2 the oxygen and iron contents are 2500 ppm and 0.3 wt%, respectively, while in grade 4 these values are 4000 ppm and 0.5%, respectively. Therefore the inconsistency in the yield strength values is due to the unclear definition of "pure titanium". It is claimed for well-annealed elemental titanium with few dislocations the yield strength value is 78.45 MPa [36]. The yield strength value of pure hcp titanium blindly predicted by the genetic algorithm is 88.5 MPa. It should be noted that this value was determined while texturing effect was ignored. Similar to room temperature hcp titanium, the yield strength value was predicted by the genetic algorithm for the pure bcc titanium which is stable at high temperatures. Since this phase is not stable at room temperature, no yield strength value reported in the literature can be

found. However, based on the fact that bcc crystal structure has more slip systems than the hcp crystal structure, it can be expected that the yield strength of the beta phase should be smaller than the alpha phase. Also yield strength values of some other well-annealed pure bcc elements are in the range of 40-84 MPa [37]. The result of the genetic algorithm optimization is in agreement with these expectations, σ_0^{β}=63 MPa. This is for the first time that σ_0^{β} is estimated.

4.3 Solid Solution Strengthening

Solid solution strengthening is the result of solute-dislocation interactions. It should be clearly noted that our equation was developed with average compositions rather than phase compositions, the latter being preferable as it more directly relates to the physics of the problem. However, this thesis relied upon a legacy database that did not have phase compositions. Efforts to estimate phase compositions using thermodynamic software such as Pandat™ were not successful and did not yield models that converged with acceptable degrees of accuracy. It is expected that the difficulty is that Pandat™ seeks equilibrium compositions, whereas our material, in certain cases, was far from equilibrium. Regarding solid solution strengthening, the origin of the interactions between solute atoms and dislocations can be explained as 1) electrostatic in nature 2) differences in the elastic constants of the solvent and solute and 3) interactions in the strain fields of dislocations and solute atoms [37, 38]. The latter two certainly play key roles in solid solution strengthening. It is worth noting that, in the case shown in this thesis, the asymmetry of the strain fields in hcp alpha titanium and the interactions between solute atoms in the bcc beta titanium also contribute to the solid solution strengthening.

Based on the regression analysis on the effect of elements on the yield strength of titanium, it can be said that O and Co has the highest and lowest effects, respectively [39].

According to this paper, the influence of O, Fe, Al, and V on the yield strength of titanium can be ranked as O>Fe>Al>V. This trend was seen in article paper as well [13].

4.4 HCP Alpha Titanium

While it is well known that Al and O significantly affect the yield strength values of titanium alloys, there is no mechanism-based or quantified study on the effect of these elements on the yield strength values of titanium alloys. According to equation 4.2, the precursors A and exponentials n were determined to be A_O=724 MPa, n_O=0.6, A_{Al}=148.5 and n_{Al}=0.63. The exponent terms are consistent and lie in the range of the two classical solid solution exponential fitting parameters, n=0.5-0.67. For directly assessing the precursor values, there is no reported value in the literature. However, based on the intrinsic flow stress of pure titanium and data presented in [40], it is possible to estimate A_{Al} to be around 160 MPa. Based upon difference in the yield strength values and oxygen content of different grades of commercially pure titanium, it can be concluded that A_O is larger than 500 MPa. It is interesting to note that these values are consistent with blindly extracted values by genetic algorithm.

The potential origin of a very strong influence of oxygen content on the yield strength values can be explained in the following manner. The common reason proposed for solid solution strengthening in hcp materials by an interstitial atom, e.g. oxygen, is the asymmetric strain fields or tetragonal distortion induced by occupying interstitial positions and deviating the c/a ratio from its ideal value. However, this is not the cause of solid solution strengthening in Ti, Zr and Hf [38]. For this group of elements, it is believed that short-range interactions between the solute atom and dislocation cause the solid solution strengthening. Initially, the <a> dislocation dissociates as follow:

$$\frac{1}{2}<11\bar{2}0>=\frac{1}{8}<22\bar{4}1>+\frac{1}{8}<22\bar{4}\bar{1}>$$

This dissociation moves the dislocation position from a lattice position occupied by Ti (or substitutional Al) to an interstitial lattice position. Prior to dislocation dissociation and stacking fault formation, the interstitials site is an octahedral site. Simple calculation considering only size of the atoms shows that for atomic radii greater than 58 pm (r_{oxygen}=60 pm), the interstitial atom occupies the octahedral site. This is in agreement with calculations which show that in Ti alloys, the octahedral site is a more energetically favored position for oxygen to occupy [39]. Due to the movement of A layer over B layer and formation of stacking faults, the interstitial site occupied by oxygen becomes an unstable tetrahedral site. Since there is not enough room for oxygen in this tetrahedral site, it moves toward the basal plane to occupy the hexahedral site and at an energy cost of +1.19 eV [39, 40]. If oxygen tends toward nonmetallic bonding (e.g., either covalent or ionic), the octahedral site is also energetically favored. The larger space, i.e., the octahedral site, is more favorable because the nature of bonding changes the oxygen size and makes it bigger. This subject is more discussed in terms of changing the density of states of the 2s and 2p orbitals in octahedral and hexahedral sites.

As discussed above, dislocation dissociation changes an octahedral site to a tetrahedral site. There would necessarily be an energy penalty for changing the location of oxygen from an octahedral site to a tetrahedral site. Also the lattice strain would be considerable for changing the position from an octahedral site to a tetrahedral site. Therefore, it can be said that the octahedral site repels the partial dislocation which approach it. It is noted that this discussion is strictly limited to <a>-type dislocations on basal planes, and does not capture physics associated with <a+c>-type dislocations or <c>-type dislocations.

4.5 Intrinsic Flow Strength

In the proposed equation (equation 4.1), it was not predetermined whether the two beta stabilizer elements (V and Fe) would have any synergistic interaction. In this case, three new variables were defined, n_1, n_2 and n_3. Such synergistic interactions between elements in one phase and their effect on the solid solution strengthening are not well understood, resulting in different models which have been previously proposed [42]. For example, one of the proposed model of solid solution strengthening of Mo and W in Nb is $\Delta\tau = \Delta\tau_1 + \Delta\tau_2$ where $\Delta\tau_1$ and $\Delta\tau_2$ are the solution strengthening values of Mo and W in Nb, respectively. In this model, it is assumed that 1) both solutes act as obstacles of the same strength and 2) yield strength is a linear function of solute concentration. However, when random or dilute array of weak or moderate obstacles interact with each other, the relation between the solute content and the yield strength can be $\sigma_{SS,tot}=\Delta\tau\sim(\sigma_{ss,A}^2+\sigma_{ss,B}^2)^{0.5}$[43]. For fcc crystal structures with $\Delta\tau_i \alpha C_i^{2/3}$ and with obstacles of equivalent strengths the synergistic contributions follows: $(\Delta\tau_1^{2/3}+\Delta\tau_2^{2/3})^{3/2}$. If synergistic effects are absent, a new model exists where the combined effect is given by: $\Delta\tau = (\sum_i \Delta\tau_i^{1/n})^n$. Note that this model will revert to the first model where interactions are present if n=1/2. The genetic algorithm has determined an optimum equation of the form $\sigma_{SS,tot}\sim(\sigma_{ss,A}^{0.445}+\sigma_{ss,B}^{0.51})^{2.06})$. Here, n~2. More completely, the precursors (A) and exponentials *n* have been determined to be A_V =49.8 MPa, n_V =0.72 MPa, A_{Fe}=179.82 MPa and n_{Fe}=0.87. Based on the genetic algorithm results and the previous discussion of interactions, there is no obvious synergistic effect between V and Fe. The significant difference in A_{Fe} and A_V shows that these two elements contribute to the strengthening differently. The possible reason is that the

dilute solution assumption is no longer valid and the concentration of the solute elements exceeds 10%.

For all the four elements, it can be said that

1. The precursors can be sorted as $A_O > A_{Fe} > A_{Al} > A_V$. This order is fully consistent with the results in the literature [13, 41].

2. Fe contributes to the yield strength significantly. The shear modulus difference between Ti and Fe is 82 GPa and this value for Ti and V is 47 GPa. In addition, there is a notable size difference. These two differences may explain the observed difference in precursor for V and Fe.

3. The average value of the exponent term n of Fe and V is greater than Al and O. This term is related to the atom-normalized influence of a solute atom on yield strength. A single atom in bcc is surround by 8 atoms (only nearest neighbors are considered) while in hcp it is surrounded by 12 atoms. Therefore, one might argue that a single atom in the bcc crystal structure can influence the slip plane more than close-packed crystal structures.

Clearly, solid solution strengthening appears is the most dominant contributor to strength in α/β processed Ti-6Al-4V alloys.

4.6 Constrained Beta Estimate

This term is presented after previous presentations by Viswanathan and Fraser have showed that the earliest dislocation activity in α/β titanium alloys occurs in the bcc beta phase. Their works showed that the dislocation activity in a thick beta rib would become arrested at a point where a single thick beta rib would bifurcate into two thinner beta ribs. This observation was fully consistent with expectations that highly constrained phases would exhibit greater strength than an unconstrained crystal of the same material and composition. This paper has sought to include the often cited α-lath thickness effect as well as the neglected but coupled beta rib thickness effect. For a fixed volume fraction of phases, as the alpha laths become thinner, the beta ribs necessarily become thinner. The previous work by Viswanathan and Fraser showing

that deformation begins in the beta phase encouraged us to consider this as a contribution to the equation. The precursor constant of 16.5 for the constrained beta term indicates this term is a significant contribution.

4.7 Monte Carlo

The lowest and highest yield strength values of the phenomenological equation were determined using the Monte Carlo method. The results of neural networks which contain error bar were compared to the genetic algorithm results after applying the Monte Carlo method. This comparison helps us understand how close two methods of prediction, neural network and genetic algorithm, are. These results are shown in fig. 4.5(a-d) to 4.8(a-d).

(a)

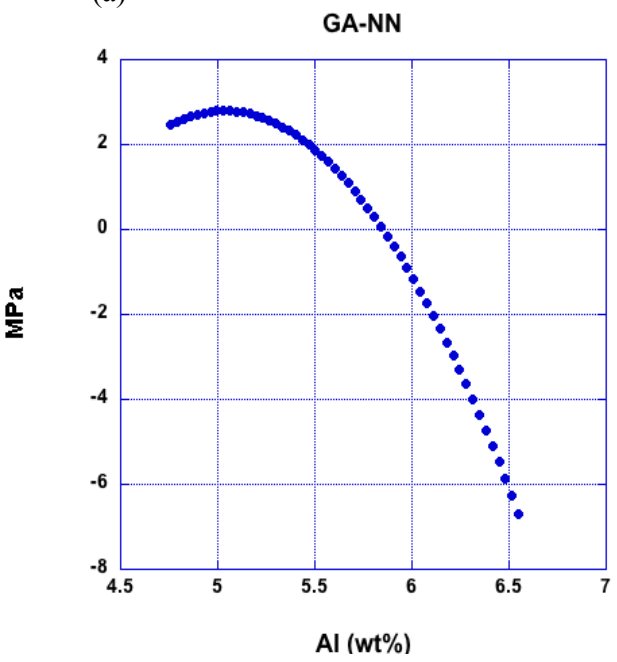

(b)

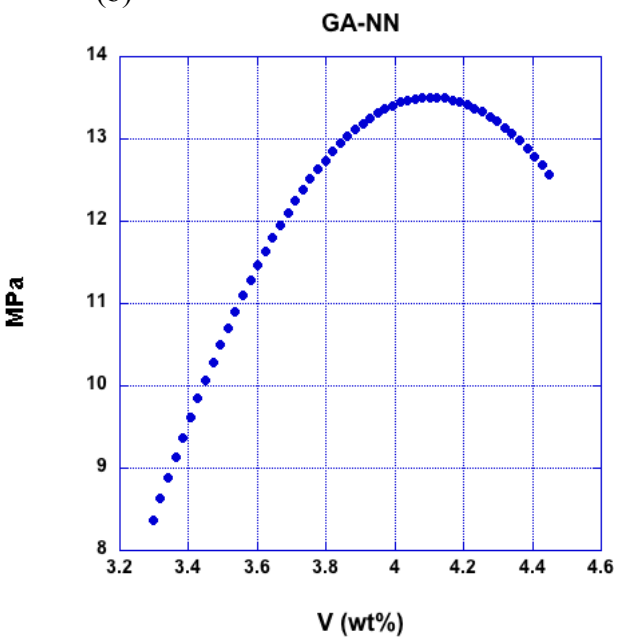

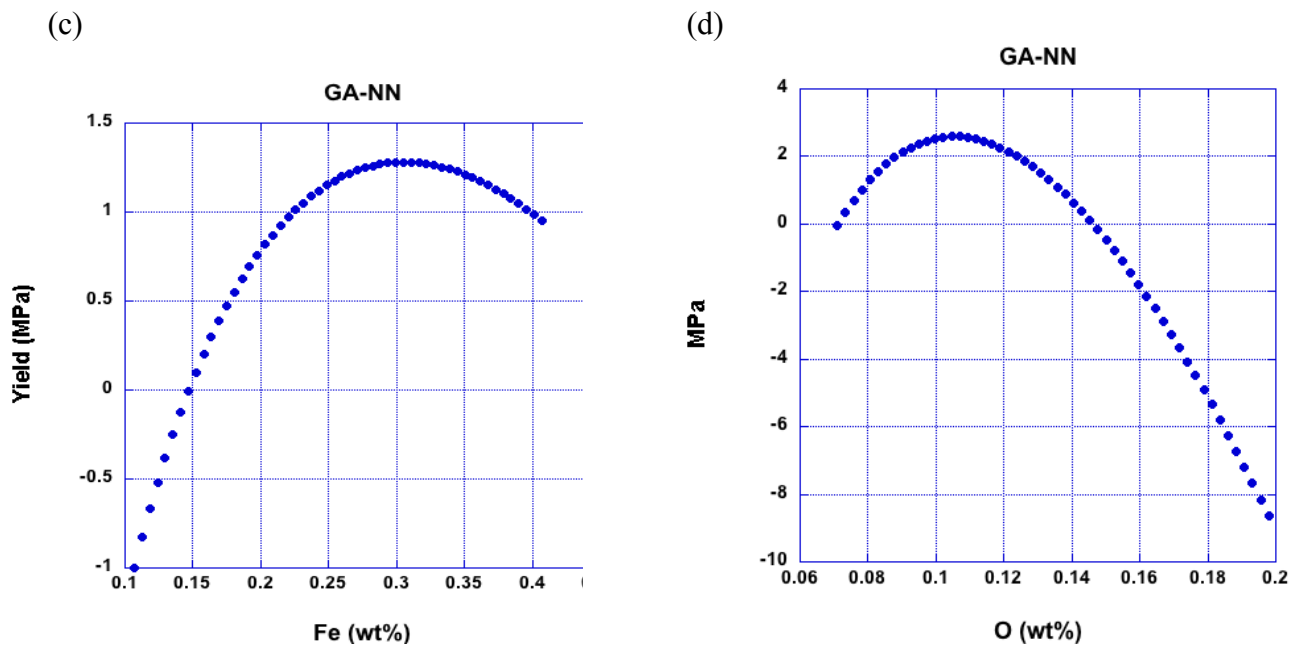

Figure 4.5. The difference between the genetic algorithm predictions and neural network predictions for (a) Al, (b) V, (c) Fe and (d) O (wt%) is shown.

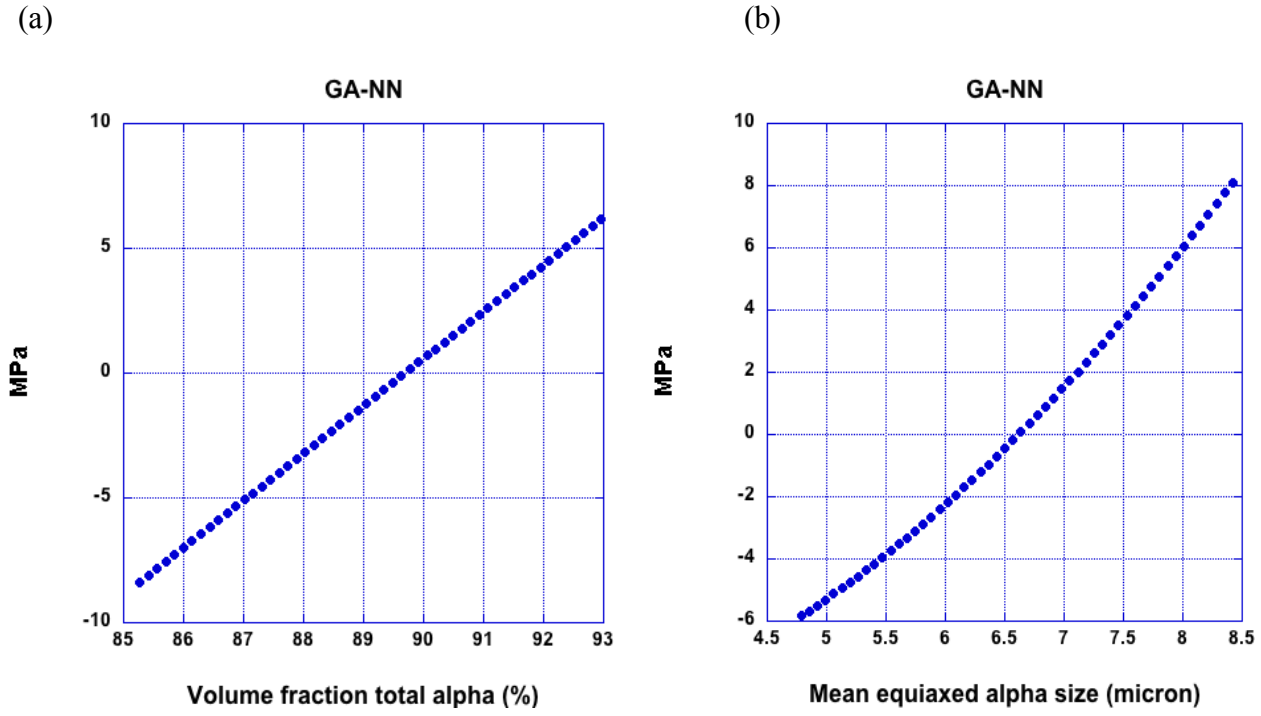

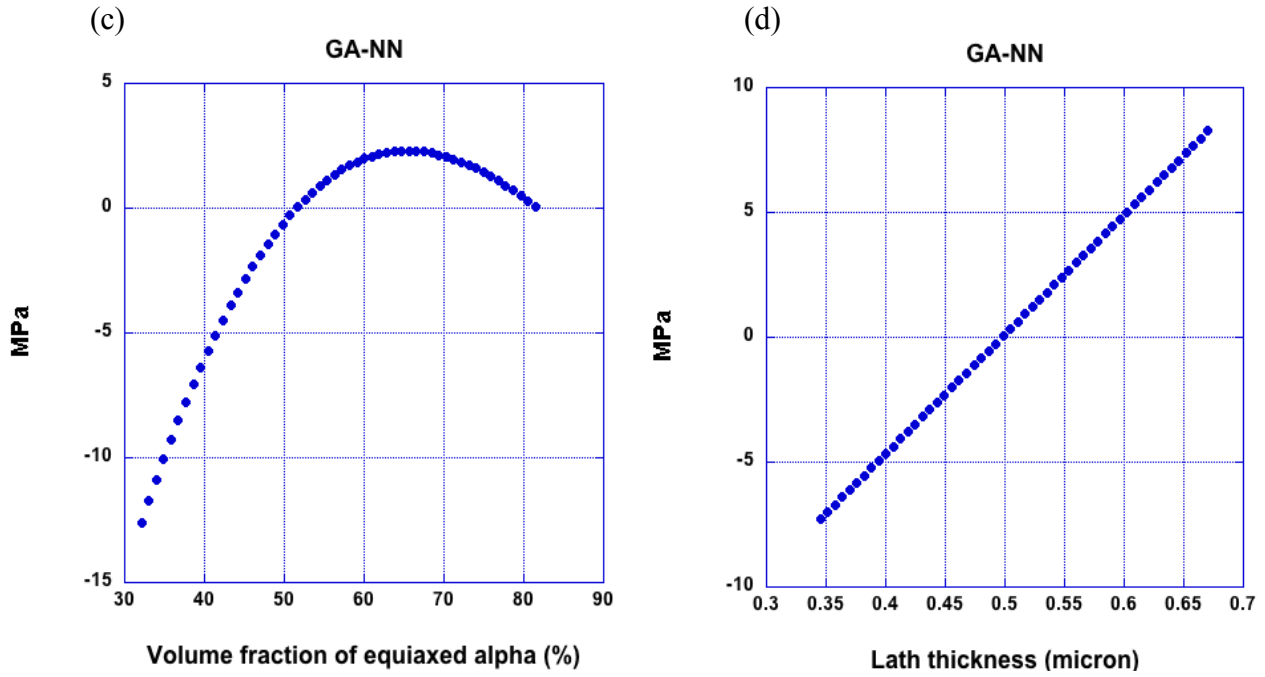

Figure 4.6. The difference between the genetic algorithm predictions and neural network predictions for (a) volume fraction total alpha (%), (b) mean equiaxed alpha size (μm), (c) volume fraction of equiaxed alpha (%) and (d) lath thickness (μm) is shown.

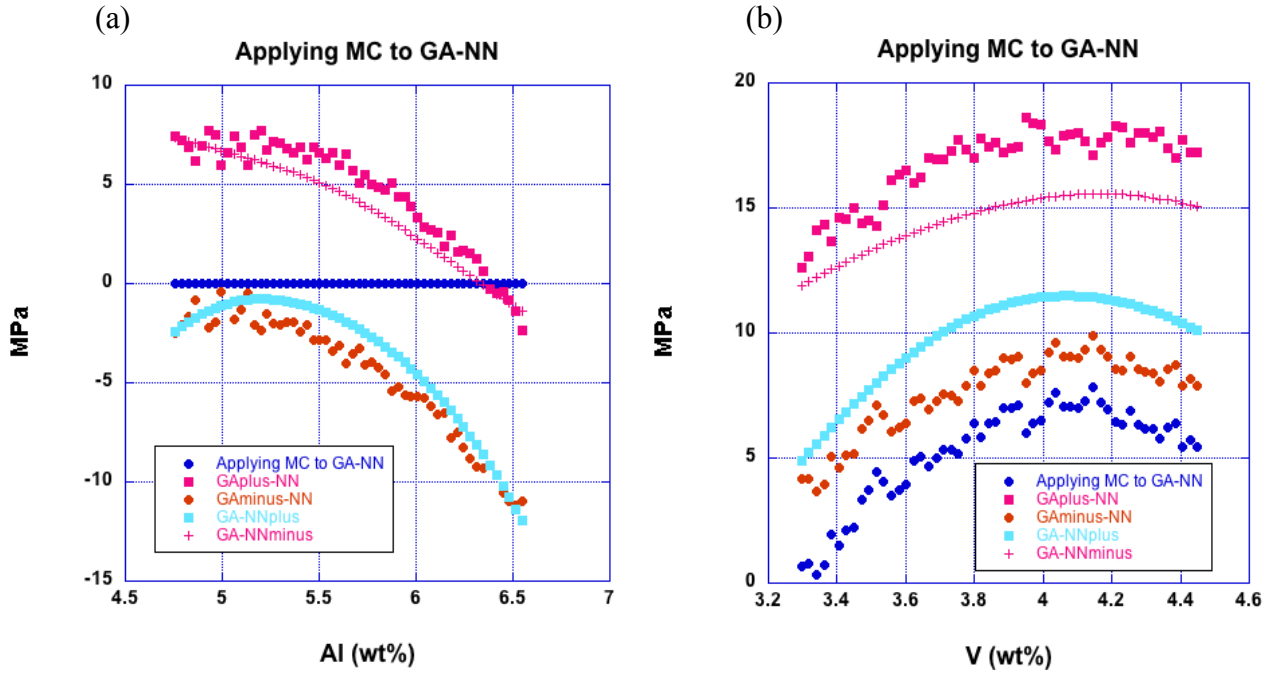

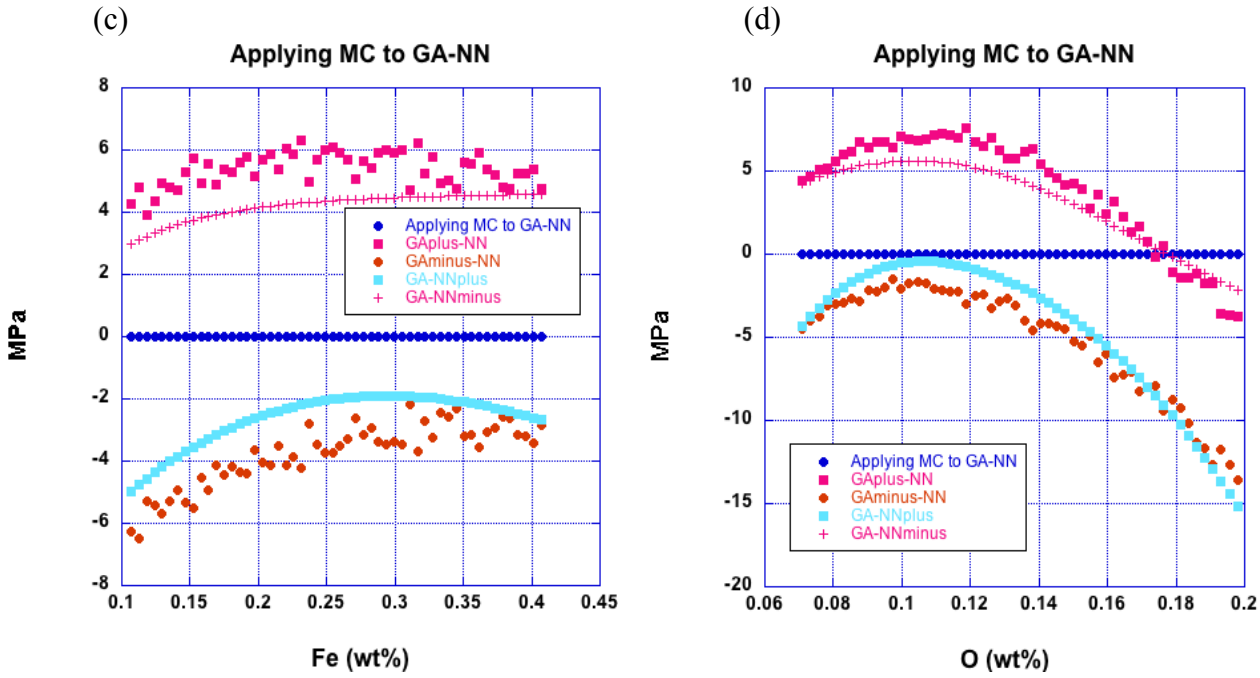

Figure 4.7. The difference between the genetic algorithm predictions (after applying the Monte Carlo method) and neural network predictions for (a) Al, (b) V, (c) Fe and (d) O (wt%) is shown.

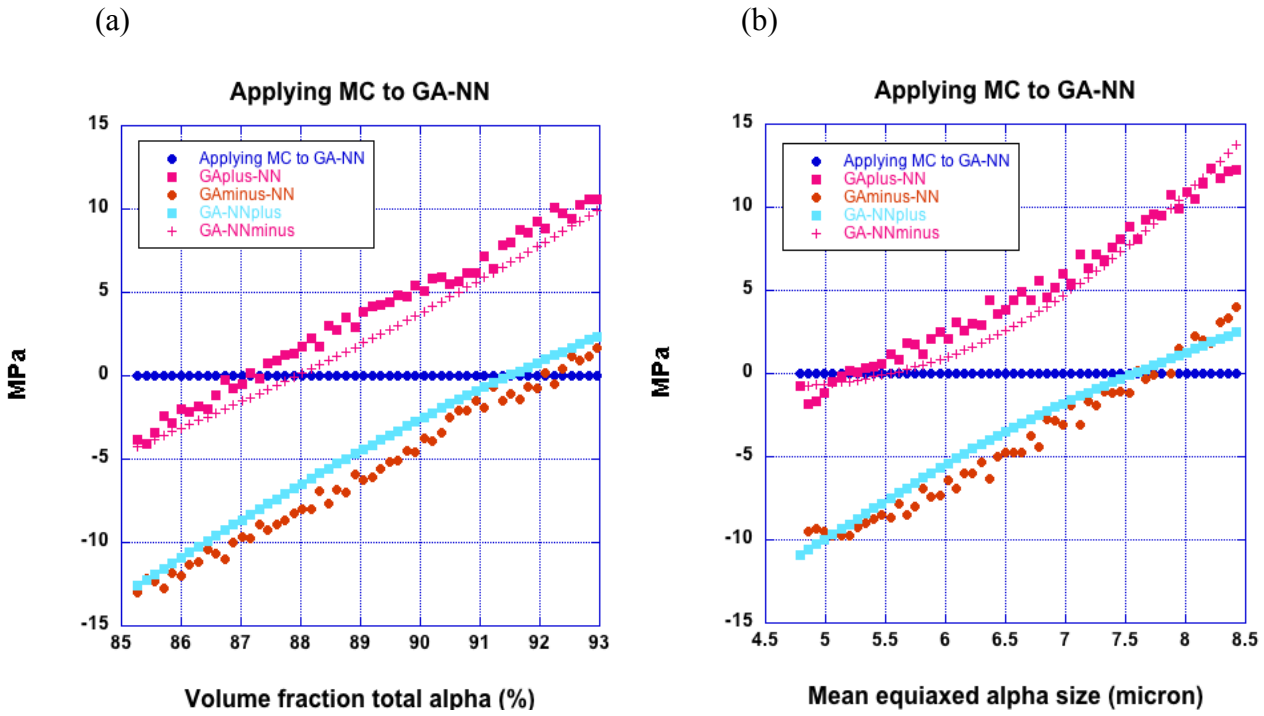

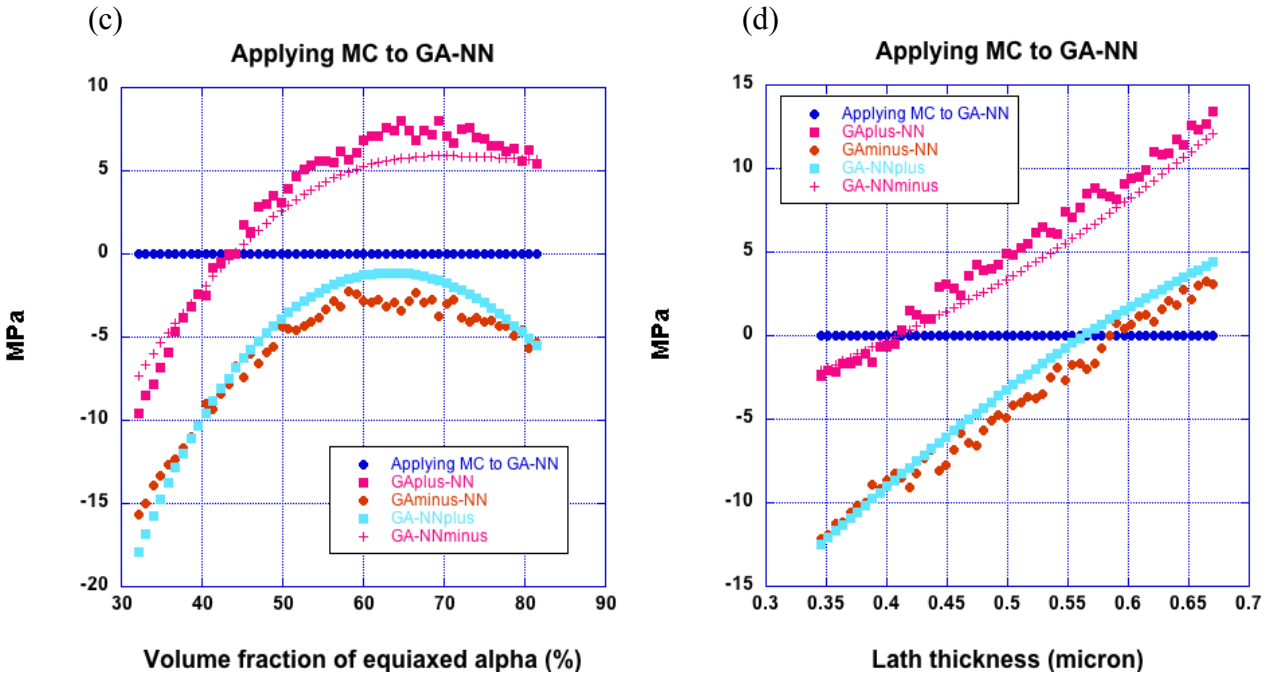

Figure 4.8. The difference between the genetic algorithm predictions (after applying the Monte Carlo method) and neural network predictions for (a) volume fraction total alpha (%), (b) mean equiaxed alpha size (μm), (c) volume fraction of equiaxed alpha (%) and (d) lath thickness (μm) is shown.

CHAPTER 5

CONCLUSIONS

A novel method to derive a phenomenological equation from a multi-component multi-phase database was discussed in this thesis. The database contained 54 samples with different compositions and heat treatments. The input variables were C_{Al}, C_V, C_{Fe}, C_O, volume fraction of total alpha, the volume fraction of equiaxed alpha, mean equiaxed alpha size and lath thickness. The output was the yield strength. Due to a very complex relationship between the inputs and output, it has historically been impossible to use regression methods to determine the phenomenological equation. Neural network models are very flexible functions which are able to adjust their weights and biases in a way which they have the best fit to the database. Initially, and in the literature, neural networks were used to develop a complex mathematical model. This mathematical model was developed without having any knowledge about the physics of the problem. Based on the developed neural network model, virtual experiments were done. In the virtual experiments, functional dependency of each variable was studied by setting the values of all the variables to a fixed value and only changing one variable from the minimum value to its maximum value.

Unique to this thesis, we have integrated a powerful genetic algorithm approach to help assess proposed phenomenological equation. Thus, the next step is to propose a phenomenological equation to predict the output as a function of inputs. The proposed functions have some known terms, which are the inputs of the database, and some unknowns which are the precursors and powers of those known terms. The output of the function is the output of the database, yield strength. The precursors and powers should be determined in a way in which the difference between predicted and measured output is “the smallest”. As described, the genetic

algorithm was used as an optimization tool to find the global minimum of highly nonlinear, stochastic and discontinues functions. The same database given to the neural network was used to find the precursors and powers. After finding these unknown precursors, virtual experiments were conducted in a similar manner to the neural networks. Comparing the virtual experiment results of the neural networks and the genetic algorithms, it is possible to add/drop terms from the proposed equation to modify it. The modification should reduce the difference between the predicted results by the two methods. Finally the Monte Carlo method was used to study the effect of uncertainties in the microstructural-feature measurements on the output. It determines the statistic uncertainties in the genetic-algorithm developed equation. Therefore instead of an exact value predicted by the equation, a range of values were predicted as the possible output. It should be noted that the neural network side is also possible to provide an error bar from the variations in its weight values. The predicted results are again compared to study the effect of uncertainties on the ability of the two models to predict the outputs. It was found that the outputs of the two methods were close together for all the variables, except V case.

From the metallurgical point of view, the developed equation shows some interesting facts including:

1. Intrinsic flow stress: Based on the blindly determined values by the genetic algorithm the σ_0^{α} is 88.5 MPa. This value is in good agreement with the well-annealed value which is 78.45 MPa. With the same method, for the first time, σ_0^{β} was predicted to be 63 MPa. This prediction is also consistent with the fact that the crystal structure of the beta phase is bcc and it should be softer than the alpha phase, and is in keeping with a range for observed values for bcc structures.

2. Hardening mechanism: According to the genetic algorithm results, although grain size reduction and strengthening from the interface are involved in the proposed equation, the dominant hardening mechanism is solid solution strengthening. Also it was found that the contribution of the elements to the yield strength follows O>Fe>Al>V. The predicted results by the neural networks and genetic algorithms are very similar and they are quite in agreement with the literature results [13, 41].

From a modeling perspective, as related to physical metallurgy, there are some limitations to both the equation developed in this thesis, and the approach in general. These include:

1. Inherently, the current approach relies upon the existence of some prior legacy knowledge. The knowledge need not be related to the system of interest in particular, but should capture deformation mechanisms (or other mechanisms of interest) in a reasonably well established relationship. Thus, this effort was successful as it was largely based upon dislocation mechanisms, which are dominant in $\alpha+\beta$ processed Ti-64. However, if this has been a twin dominated deformation process (or perhaps even variations in creep behavior at higher temperatures), the development of the equation might have met with greater difficulty. We propose that a solution might be to develop an equation which contains a hyperbolic tangent function "residual" which could flexibly capture physics that are unknown.

2. As discussed, the compositions captured in the equation are average alloy compositions rather than phase compositions. This was done given the fact that this was a legacy database and not one developed specifically for this thesis. Consequently, precise measurements of phase composition could not be conducted. Attempts to model phase

composition were not effective. However, without question, it is more physically precise to describe phase compositions rather than bulk compositions.

3. The constant that describes the properties of the transformed β-phase has not been related to a physical phenomenon. It is possible that this parameter is related to the basketweave microstructure. However, this is unknown.

Finally, there are some subjects that could be considered as future works:

1. The effect of texturing was not considered in developing this equation. Therefore, it is worthy to find a way to quantify the texture values and then added a new term(s) to the equation which represents the texturing effects.

2. Vanadium is added to the material to get basketweave microstructure. The proposed equation does not have any term which represents the effect of basketweave on the yield strength. It is proposed that this missing term caused a small amount of discrepancy between the yield strength values predicted by the neural networks and the genetic algorithms for the V plot.

3. Importantly, while this equation is still somewhat limited to a particular composition and microstructure envelope (and consequently somewhat prone to extrapolative risks in its present form), the individual phenomenon are likely to be reasonable representations of reality. Thus, a key benefit of this equation is that the extension of it will likely require less populated, less expensive databases as fewer strengthening mechanisms are “truly unknown”.

BIBLIOGRAPHY

1. Lutjering, G., Property optimization through microstructural control in titanium and aluminium alloys. Materials science and engineering A, 1999. 263: p. 117-6.

2. Boyer, R., G. Welsch, and E.W. Collings, Materials properties handbook: Titanium alloys. 2007: Ohio.

3. Kar, S., et al., Modeling the tensile properties in b-processed a/b Ti alloys. Metallurgical and materials transactions A, 2006. 37A: p. 559-6.

4. Kapoor, R., D. Pal, and J.K. Chakravartty, Use of artificial neural networks to predict the deformation behavior of Zr-2.5Nb-0.5Cu. Journal pf materials processing technology, 2005. 169: p. 199-5.

5. Topçu, I.B. and M. Saridemir, Prediction of rubberized concrete properties using artificial neural network and fuzzy logic. Construction and Building Materials, 2008. 22(4): p. 532-0.

6. Cai, J., R.A. Cottis, and S.B. Lyon, Phenomenological modelling of atmospheric corrosion using an artificial neural network. corrosion science, 1999. 41: p. 2001-30.

7. Bhadeshia, H.K.D.H., Neural networks and information in materials science. Statistical analysis and data mining, 2009. 1: p. 296-5.

8. Bhadeshia, H.K.D.H., Neural networks in materials science. ISIJ international, 1999. 39(10): p. 966-79.

9. Bhadeshia, H.K.D.H., D.J.C. Mackay, and L.E. Svensson, The impact toughness of C-MN steel arc-welds - A Bayesian neural network analysis. Materials science and technology, 1995. 11: p. 1046-1.

10. Mackay, D.J.C., A practical bayesian framework for backpropagation networks. Network: computation in neural systems, 1995. 6: p. 448-72.

11. Capdevila, C., F.G. Caballero, and C.G.D. Andres, Determination of Ms temperature in steels: A Bayesian neural network model. ISIJ international, 2002. 42(8): p. 894-2.

12. Gavard, L., et al., Bayesian neural network model for austenite formation in steels. Materials cience and technology, 1996. 12: p. 453-463.

13. Collins, P.C., et al., Neural networks relating alloy composition, microstructure and tensile properties of a/b processed TIMETAL 6-4. Metallurgical and materials transaction A, 2012.

14. Cool, T., H.K.D.H. Bhadesia, and D.J.C. Mackay, The yield and ultimate tensile strength of steel welds Materials science and engineering A, 1997. 223: p. 186-00.

15. Kashyap, B.P. and K. Tangri, Hall-Petch relationship and substructural evolution in Boron containing type 316L stainless steel. Acta materialia, 1996. 45(6): p. 2383-95.

16. Tang, J., et al., Hall-Petch relationship in two-phase TiAl alloys with fully lamellar microstructures. MAterials research bulletin, 2002. 37: p. 1315-1.

17. Paradkar, A.G., et al., On the validity of Hall-Petch equation for single-phase b Ti-Al-Nb alloys undergoing stress-induced martensitic transformation. Materials science and engineering A, 2009. 520: p. 168-3.

18. Zhao, M.-C., et al., Relationship between yield strength and grain size for a bimodal structural ultrafine-grained ferrite/ cementite steel. Scripta materialia, 2007. 57: p. 857-0.

19. Dimitriu, R.C., et al., Hot-strength of ferritic creep-resistant steels Comparison of neural network and genetic programming. Materials and manufacturing processes, 2009. 24: p. 10-5.

20. Collins, P.C., et al. Design tools for structural metallic materials. in Frontiers in the design of materials (FDM-NMD-ATM). 2006. Madras, Chennai.

21. Mark, S. and S. Mordechai, Applications of Monte Carlo method in science and engineering. 2011, InTech: India.

22. Thompson, B.E., Monte Carlo simulation of ion transport through rf glow-discharge sheaths. Journal of applied physics, 1988. 63: p. 2241-2251.

23. Beaudoin, A.J., R. Srinivasan, and S.L. Semiatin. Microstructure modeling and prediction during thermomechanical processing. 2002.

24. Ding, Z.J. and H.M. Li, Application of Monte Carlo simulation to SEM image contrast of complex structures. Surface and interface analysis, 2005. 37: p. 912-8.

25. Sallabi, A.K., J.N. Dawoud, and D.B. Jack, A Monte Carlo simulation study of Nitrogen on LiF (001). Applied surface science, 2010. 256: p. 2974-8.

26. Tikare, V., M.A. Miodownik, and E.A. Holm, Three-dimensional simulation of grain growth in the presence of mobile pores. Journal of american ceramic society, 2001. 84(6): p. 1379-5.

27. Global optimization toolbox (User's guide). 2011.

28. Borradaile, J.B. and R.H. Jeal. Mechanical properties of titanium alloys. in The 4th international conference on titanium science and technology 1980. Kyoto, Japan.

29. Lutjering, G., J. Albrecht, and A. Gysler. Mechanical properties of titanium alloys. in Titanium '92: science and technology. 1993. Warrendale, USA.

30. Ambard, A., et al., Role of interphases in the deformation mechanisms of an a/b titanium alloy at 20 K. Materials science and engineering A, 2001. 319-321: p. 404-408.

31. Lutjering, G., Influence of processing on microstructure and mechanical properties of a+b titanium alloys. Materials science and engineering A, 1998. 243: p. 32-45.

32. Collins, P.C. and H.L. Fraser, Modeling of tensile properties, in ASM Handbook: Fundamentals of modeling for metals processing. 2009. p. 377-399.

33. Labusch, R., et al., Rate processes in plastic deformation of materials, in ASM handbook. 1975, 26. p. 26.

34. Gypen, L.A. and A. Deruyttere, Multi-component solid solution hardening Part 2: agreement with experimental results. Journal of materials science, 1977. 12: p. 1034-8.

35. Collins, P.C., et al., Development of methods for the quantification of microstructural features in a+b-processed a/b titanium alloys. Materials science and engineering A, 2009. 508: p. 174-2.

36. Abbaschian, R., L. Abbaschian, and R.E. Reed-Hill, Physical Metallurgy Principles. Fourth ed. 2009.

37. Tyson, W.R., Strengthening of hcp Zr, Ti and Hf by interstitial solutes- a review. Canadian metallurgical quarterly, 1967. 32: p. 301-32.

38. Wu, H.H. and D.R. Trinkle, Direct diffusion through interpenetrating networks: Oxygen in titanium. Physical review letters, 2011. 107(4).

39. Henning, R.G., et al., Impurities block the alpha to gamma martensitic transformation in titanium. nature materials 2005. 4: p. 129-3.

40. Ankem, S., et al. Multiple regression analysis of the effects of various alloying elements on the properties of titanium alloys. In Sixth world conference on titanium. 1988. France